The Oxy-CaL process: A novel CO_2 capture system by integrating partial oxy-combustion with the Calcium-Looping process

C. Ortiz [a, *], J.M. Valverde [a], R. Chacartegui [b], M. Benítez-Guerrero [a, c], A. Perejón [c, d], L.M. Romeo [e]

[a] Facultad de Física, Universidad de Sevilla, Sevilla, Spain
[b] Escuela Técnica Superior de Ingeniería, Universidad de Sevilla, Sevilla, Spain
[c] Instituto de Ciencia de Materiales de Sevilla (C.S.I.C.-Univ. Sevilla), Sevilla, Spain
[d] Departamento de Química Inorgánica, Facultad de Química, Universidad de Sevilla, Sevilla, Spain
[e] Escuela de Ingeniería y Arquitectura, Departamento de Ingeniería Mecánica, Universidad de Zaragoza, Spain

* Corresponding author. Tel.: +34 655783930
E-mail address: cortiz7@us.es

Abstract

This paper proposes a novel CO_2 capture technology from the integration of partial oxy-combustion and the Calcium Looping capture process based on the multicycle carbonation/calcination of limestone derived CaO. The concentration of CO_2 in the carbonator reactor is increased by means of partial oxy-combustion, which enhances the multicycle CaO conversion according to Thermogravimetric analysis results carried out in our work, thus improving the CO_2 capture efficiency. On the other hand, energy consumption for partial oxy-combustion is substantially reduced as compared to total oxy-combustion. All in all, process simulations indicate that the integration of both processes has potential advantages mainly regarding power plant flexibility whereas the overall energy penalty is not increased. Thus, the resulting energy consumption per kilogram of CO_2 avoided is kept below 4 MJ/kg CO_2, which remains below the typical values reported for total oxy-combustion and amine based CO_2 capture systems whereas CO_2 capture efficiency is enhanced in comparison with the Calcium Looping process.

Keywords: Calcium-Looping, oxy-combustion, CCS, SPECCA

1. Introduction

Carbon Capture and Storage (CCS) is considered as one key strategy to mitigate global warming [1,2]. In order to achieve a commercial deployment of post-combustion CO_2 capture in fossil fuel power plants, several technologies are being analyzed aimed mainly at maximizing the capture efficiency while energy penalty and capital cost are minimized [3,4]. Among diverse possibilities, already commercial amine-based capture systems and the Calcium-Looping (CaL) process, currently under pilot-scale stage, have attracted a great deal of attention in the last years [5,6]. Although CO_2 capture by using MEA (monoethanolamine) is an industrial mature process, its commercial deployment as post-combustion CO_2 capture technology is hampered by the high energy penalty (8-12%) mainly due to sorbent regeneration [7–9], amine toxicity [10] and degradation [11].

The CaL process is based on the carbonation/calcination reaction of solid CaO particles, which is carried out in two interconnected circulating fluidized bed (CFB) reactors [12]. This second generation capture technology has several potential advantages when compared with amine-based process such as a lower energy penalty over the power plant (4-9%) [6], higher CO_2 capture efficiency (above 90%) and the use of low cost, widely available and non-toxic natural minerals as CaO precursors such as limestone or dolomite [13]. Even though several pilot scale plants (~ 1-2 MW_{th}) are already showing promising results [14,15] the CaL technology has not reached a demonstration stage yet. The main causes that hinder such step forward are linked to the excessively large size of the capture system (carbonator reactor height ~ 40 m; carbonator solids inventory ~ 400 ton; additional coal consumption for CO_2 capture ~ 45-55%), which increases significantly both capital and operating costs (CAPEX and OPEX) for power generation [16,17].

Another interesting possibility to mitigate CO_2 emissions from power plants is the oxy-combustion technology, which has been successfully demonstrated in large-scale pilot projects (30 MW_e) [18–20]. Essentially, oxy-combustion consists of replacing air by pure O_2 (mixed with CO_2-rich flue gas recycled) as combustion gas, which yields a highly-concentrated CO_2 flue gas stream. After purification, the CO_2 stream (~95% vol) is suitable for compression and storage or utilization [21]. The main drawback for the large-scale deployment of oxy-combustion is the high energy consumption for pure O_2 production in the cryogenic Air Separation Unit (ASU), which causes an energy penalty in the range of 7–13% [22,23] or, equivalently, over 20% additional fuel consumption for power production.

In this paper a novel system (Oxy-CaL) for CO_2 capture is investigated based on the combination of partial oxy-combustion and the CaL process with the goal of exploiting the synergies between such technologies. Basically, Oxy-CaL consists of carrying out a partial oxy-combustion process to produce a flue gas with a CO_2 concentration in the range 30-60% vol, which is then sent to the CaL capture process. In a similar way, other authors have analyzed the integration of partial oxy-combustion and MEA [24], which is expected to help mitigating MEA degradation and energy consumption.

The manuscript starts by showing experimental results from a thermo-gravimetric analysis (TGA) on the multicycle conversion of limestone derived CaO under realistic calcination conditions (high temperature and high CO_2 concentration). In these TGA tests, the CO_2 concentration in the carbonation environment was varied in the range 15-60% vol in order to address the effect of an excess of CO_2 in the carbonator over the typical vol% in the flue gas at typical combustion conditions (~15%). Moreover, the carbonation temperature was varied in the range 625-680ºC, which affects critically the carbonation kinetics in the solid-state diffusion-controlled stage as will be seen. These TGA results are used afterwards in the Oxy-CaL integration model to calculate the CO_2 capture efficiency from process simulations. The energy penalty arising from the diverse CO_2 capture technologies considered (total oxy-combustion, CaL and Oxy-CaL) is analyzed. Finally, the oxy-CaL performance is assessed and compared with those of other CO_2 capture systems.

Our results show that the Oxy-CaL system is a promising hybrid concept to be applicable in new power plants, allowing for a substantial reduction of energy penalty as compared to total oxy-fuel combustion. Moreover, the Oxy-CaL system leads to a high CO_2 capture efficiency in comparison with the CaL process, which would serve to reduce significantly the carbonator reactor size.

2. Thermogravimetric analysis

a. Materials and Methods

The material employed in this work was natural limestone of high purity (99.6%wt $CaCO_3$), received from Segura S.L (Matagallar quarry, Pedrera, Spain). Carbonation/calcination multicycle tests were carried out using a thermogravimetric analyzer TGA Discovery (TA Instruments 2011) equipped with an infrared halogen lamp furnace wherein the lamps are placed symmetrically with respect to a SiC enclosure to minimize undesired heat transfer phenomena. This setup allows for high heating/cooling rates (300ºC/min), which is a necessary requirement to mimic realistic conditions in the CaL process where the solids are rapidly circulated between the reactors. The TGA instrument is also equipped with a high sensitivity balance (<0.1 μg) characterized by a small baseline dynamic drift (<10 μg). A thermocouple is located close to the sample and underneath it for a reliable measurement and control of temperature in the sample.

TGA experiments consisted of 20 carbonation/calcination cycles preceded by a precalcination of the sample at 950ºC for 5 minutes under a 30% air/70% CO_2 vol/vol. atmosphere. Then, the temperature is decreased at 300ºC/min to introduce the carbonation stage at the desired temperature and under a given CO_2/air mixture. After that, the sample is calcined for CaO regeneration by quickly increasing the temperature at 300ºC/min to 950ºC under a high CO_2 concentration environment (30% air/70% CO_2 vol/vol.) as representative in the calciner environment [25,26]. Short residence times of 5 minutes for both calcination and carbonation stages have been employed as corresponds to realistic conditions. In order to mimic the integration of the CaL process with oxy-fuel combustion (Oxy-CaL), four different CO_2/air mixtures were tested for the carbonation stage: 15% CO_2/85% air, 30% CO_2/70% air, 45% CO_2/55% air and 60% CO_2/40% air (vol/vol). Three different carbonation temperatures (625ºC, 650ºC and 680ºC) were used. Tests are labeled as CaL-T for those in which carbonation was performed under 15% CO_2, where T stands for the carbonation temperature, and Oxy-CaL-vol-T, where vol is the vol% of CO_2 in the CO_2/air mixture and T is the carbonation temperature. Samples of small and fixed mass (~10 mg) were employed to avoid mass transfer resistance within the sample. Intraparticle pore diffusion limitations on the reaction rate are also avoided by using particles of size below 100 μm [27,28].

b. Experimental results and discussion

Figure 1 shows examples of thermograms obtained for the 1st (Figure 1a) and 20th (Figure 1b) carbonation/calcination cycles under CaL (15% vol CO_2 carbonation) and Oxy-CaL (30%, 45% and 60% vol CO_2 carbonation) conditions. These thermograms show the time evolution of

temperature and sample mass % along the cycles and illustrate already an important effect of raising the carbonation CO_2 vol concentration on the reaction kinetics. As well-known from previous studies CaO carbonation is seen to take place along two well-differentiated stages [29–31]. The first stage consists of a reaction-controlled fast phase on the surface of the particles that ends up when a 30-50 nm thick carbonate layer is built up on the CaO surface [29]. This first phase is followed up by a second slower phase limited by the solid-state diffusion of CO_3^{2-} mobile ions and counter-current diffusion of O^{2-} anions across the $CaCO_3$ product layer [31,32]. As may be seen in Figure 1, carbonation in the fast phase is markedly enhanced as the CO_2 concentration is increased, whereas, on the contrary, diffusion-controlled carbonation is markedly hindered. Thus, carbonation in the diffusion-controlled stage contributes significantly to the overall capture capacity under CaL conditions but loses relevancy as the CO_2 vol% is increased. As will be seen from process simulations this effect on the carbonation kinetics has remarkable implications on the role of key process operation parameters such as the solids residence time in the carbonator.

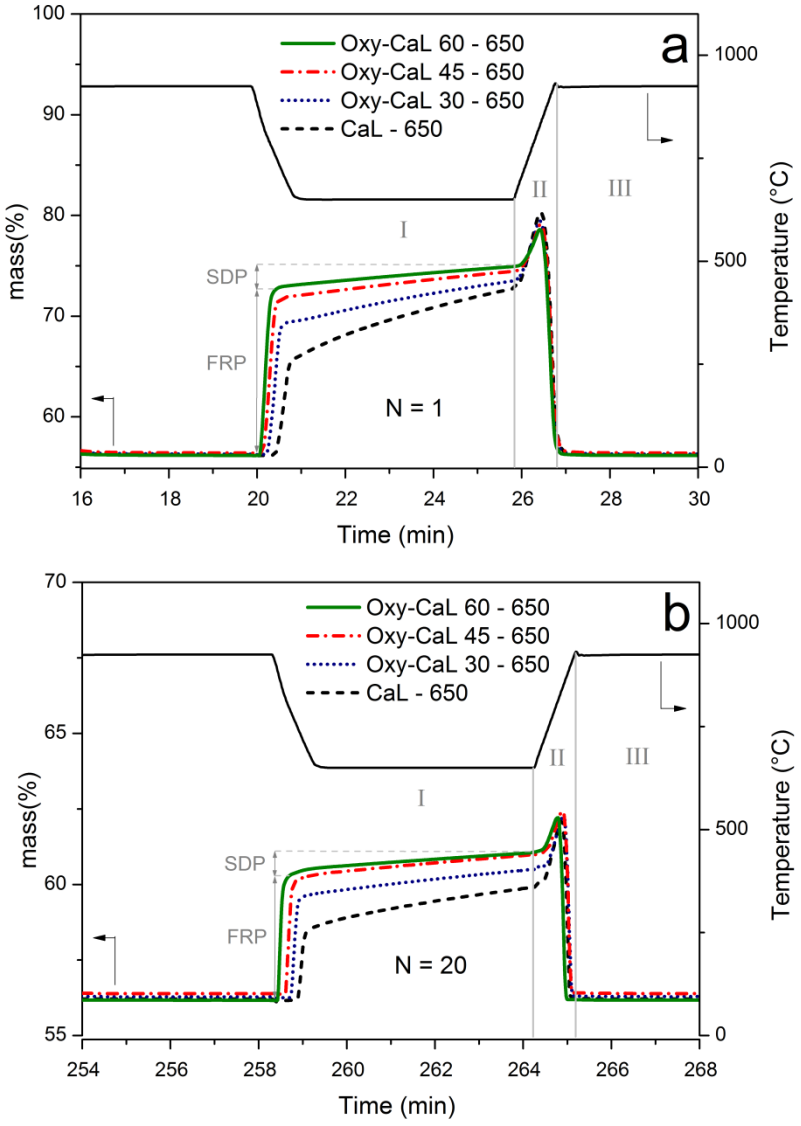

Figure 1. Time evolution of the sorbent mass % during the carbonation and calcination stages in the a) 1st cycle (N=1) and b) 20th cycle (N=20) for limestone tested under CaL (15% vol CO_2 carbonation) and Oxy-

CaL (30%, 45%, 60% vol CO_2 carbonation) conditions. Carbonation temperature is fixed to 650ºC. I indicates the carbonation stage, II the transition stage and III the calcination stage. Mass gain in the two phases of carbonation (fast reaction-controlled phase FRP and solid-state diffusion controlled phase SDP) are indicated.

Figure 2a shows the thermograms corresponding to the 1st cycle obtained from TGA tests performed at different carbonation temperatures (625, 650 and 680ºC) under CaL conditions (15% vol CO_2 carbonation). As may be observed, a variation of just about 25ºC around the typical carbonation temperature used in pilot-scale plants (~650ºC) has a significant effect on the CO_2 uptake in the diffusion-controlled stage, which notably affects the overall capture capacity. Thus, carbonation in this phase is enhanced with temperature while a decrease of the carbonation temperature yields a rapid decay of the carbonation rate in this solid-state diffusion-controlled stage. This result is consistent with the strong dependence on temperature measured elsewhere for C^{14} isotope diffusivity in CaO and for the effective product layer diffusivity of CO_3^{2-} mobile ions in the range of carbonation temperatures used in our work [30,33]. A similar behavior has been observed for the samples tested under Oxy-CaL conditions. Nonetheless, the variation with the temperature of the CO_2 capture capacity in the diffusion-controlled stage plays a relatively minor role on the overall capture capacity under Oxy-CaL conditions as compared to CaL conditions. This may be seen in Figure 2b, which shows the 1st cycle of the thermograms obtained under different carbonation temperatures for the sample tested under Oxy-CaL 45 conditions.

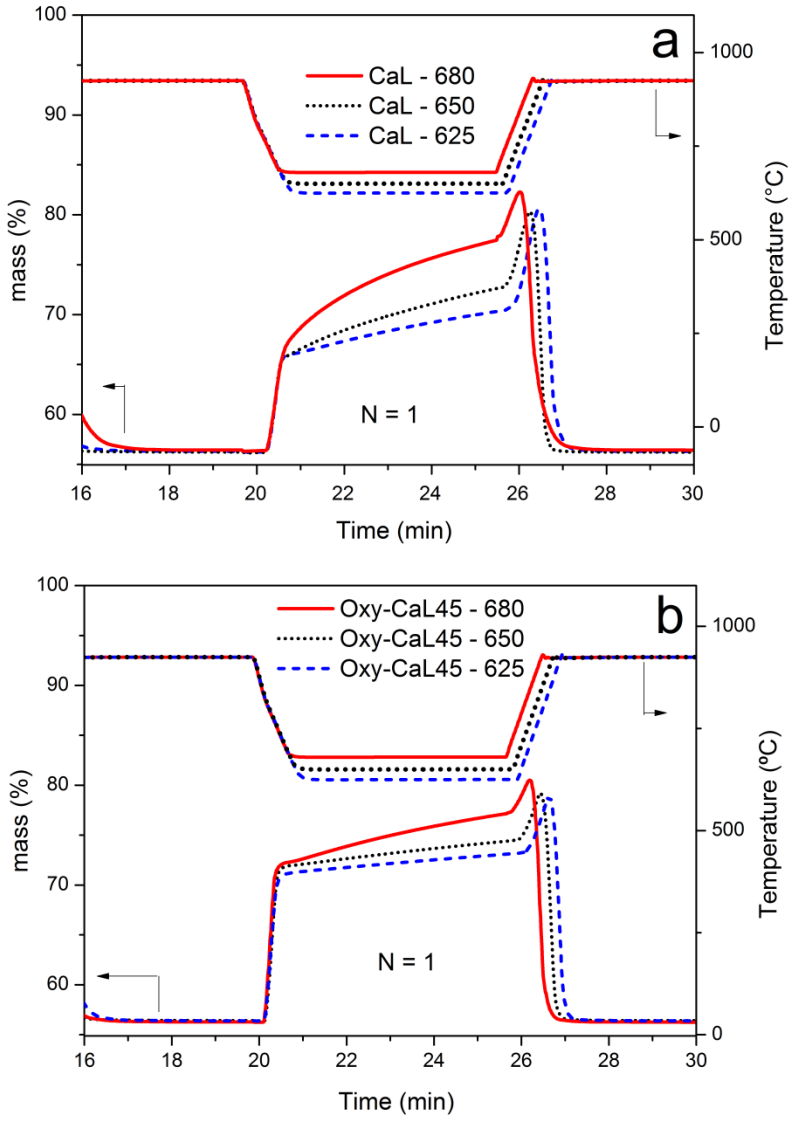

Figure 2. Time evolution of the sorbent mass % during the 1st cycle (N=1) for limestone under (a) CaL (15% vol CO_2 carbonation) and (b) Oxy-CaL 45 (45% vol CO_2 carbonation) conditions for different carbonation temperatures (625ºC, 650ºC and 680ºC) as indicated.

The parameter used to compare the multicycle capture performance of limestone under CaL and Oxy-CaL conditions is CaO conversion, defined as the ratio of CaO mass converted to $CaCO_3$ in the carbonation stage of each cycle to the sorbent mass before carbonation. Multicycle CaO conversion data can be generally well fitted by the following semi-empirical equation [6,34,35]:

$$X_N = X_r + \frac{X_1}{k(N-1) + \left(1 - \frac{X_r}{X_1}\right)^{-1}}; \quad (N = 1, 2, \ldots.) \qquad (1)$$

where N is the cycle number, X_1 is CaO conversion at the first cycle, k is the deactivation rate constant and X_r is the residual CaO conversion. Figure 3a shows multicycle CaO conversion

data and best fit curves from equation (1) for the samples tested under CaL and Oxy-CaL conditions for a carbonation temperature of 650ºC. Best fitting parameters are summarized in Table 1. As well known, CaO conversion decreases progressively with the cycle number due to enhanced grain sintering in the calcination stage at high temperature and under high CO_2 partial pressure [6,36,37], which reduces the CaO surface area available for fast carbonation in each cycle. Note however, that the deactivation rate is decreased as the CO_2 concentration in the carbonation stage is increased. Thus, the residual conversion X_r takes values of 0.062, 0.070, 0.076 and 0.081 for the samples tested under CaL-650, Oxy-CaL 30-650, Oxy-CaL 45-650 and Oxy-CaL 60-650 conditions, respectively.

The relative contributions to the overall CaO conversion of the fast reaction controlled phase (FRP) and solid-state diffusion controlled phase (SDP) have been analyzed by extracting from the thermograms the values of CaO conversion in each one of these phases (X_{FRP} and X_{SDP}, respectively, see Figure 1a). Data on X_{FRP} and X_{SDP} are shown in Figure 3b and Figure 3c. As was inferred from Figure 2, it is seen that X_{FRP} becomes increasingly relevant while X_{SDP} is decreased as the CO_2 concentration in the carbonation environment is increased.

Table 1: Values of the deactivation rate constant κ and residual conversion X_r obtained from the best fits of Eq. (1) to TGA experimental data for carbonation at different CO_2 concentrations (15% vol in the CaL tests; 30%, 45%, and 60% vol in the Oxy-CaL tests).

T carb =650ºC		**CaL-650**	**Oxy-CaL30-650**	**Oxy-CaL45-650**	**Oxy-CaL60-650**
X_N	X_1	0.373	0.388	0.407	0.425
	κ	0.731	0.667	0.651	0.633
	X_r	0.061	0.070	0.076	0.081
	R_{sqr}	0.999	0.999	0.999	0.999
X_{FRP}	X_1	0.207	0.293	0.344	0.374
	κ	0.660	0.661	0.641	0.674
	X_r	0.037	0.053	0.060	0.068
	R_{sqr}	0.999	0.999	0.999	0.998
X_{SDP}	X_1	0.166	0.095	0.063	0.051
	κ	0.828	0.686	0.711	0.633
	X_r	0.025	0.016	0.016	0.014
	R_{sqr}	0.998	0.998	0.993	0.980

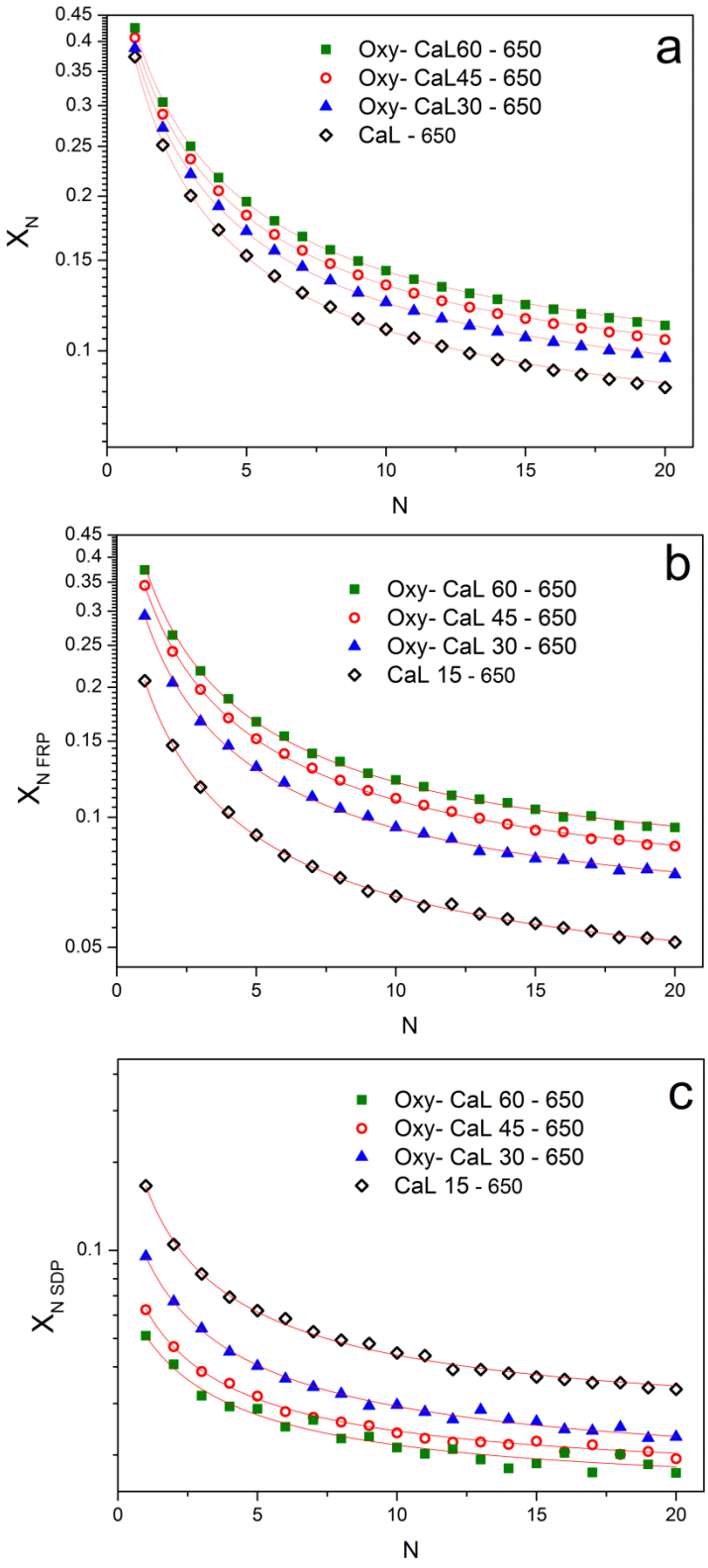

Figure 3. (a) CaO conversion versus cycle number for carbonation/calcination tests carried out under CaL and Oxy-CaL conditions. (b) Conversion in the fast reaction controlled phase. (c) Conversion in the solid-state diffusion phase. Carbonation is carried out at 650ºC under 15% vol CO_2 (CaL) and 30% vol, 45%CO_2 and 60% vol CO_2 for the Oxy-CaL tests as indicated. Calcination in all the tests is performed at 950ºC (70% CO_2/30% air vol/vol). Solids lines are the best fits of equation 1 to data.

The effect of varying the carbonation temperature around 650ºC on the multicycle CaO conversion performance for the different CaL and Oxy-CaL conditions was also investigated in our work. Data on the multicycle CaO conversion (X_N, X_{FRP} and X_{SDP}) for the tests carried out under CaL and Oxy-CaL-45 conditions at 625, 650 and 680ºC are shown in Appendix A. The results show that the overall conversion increases with the carbonation temperature while conversion in the fast reaction controlled phase is essentially independent of the carbonation temperature in the range of temperatures tested. The main effect of varying the carbonation temperature is therefore observed on the conversion in the solid-state diffusion controlled phase, which is significantly enhanced with the carbonation temperature (see Figure 15c and Figure 15f in Appendix A). A similar behavior was observed for the samples tested under Oxy-CaL-30 and Oxy-CaL-60 conditions.

3. The Oxy-CaL process

a. Description

The Oxy-CaL process newly proposed in the present manuscript is a CO_2 capture hybrid system based on the combined use of partial oxy-combustion and the CaL capture process. The basic idea behind Oxy-CaL is to exploit the enhancement of CO_2 capture capacity in the CaL process as the CO_2 concentration in the carbonation environment is increased (as seen above from the TGA tests) whereas the energy penalty for partial oxy-combustion to increase the CO_2 concentration in the flue gas is notably reduced as compared to total oxy-combustion. Figure 4 shows a schematic representation of this integration as applied to CO_2 capture in a coal fired power plant (CFPP).

As can be seen in Figure 4, the Oxy-CaL process is initiated by partial oxy-combustion of coal using to this end a mixture of air, nearly pure oxygen (purity ≥95%) and CO_2-enriched recycled flue gas at combustor temperatures between 850ºC and 950ºC. As a result, the flue gas stream exiting the boiler reaches a CO_2 vol concentration in the range 30–60% (depending on the air/O_2/CO_2 mixture composition) instead of the typical 15% vol concentration obtained from combustion with just air. The heat released by combustion is used for electric power production by means of a steam power cycle. Once partial oxy-combustion is carried out, the CO_2-enriched flue gas is sent to the CaL process. The CO_2 present in the flue gas reacts in the carbonator with a fluidized bed of CaO particles at temperatures around 650ºC. The carbonated particles are then circulated to the calciner reactor in which fast decomposition of $CaCO_3$ occurs to regenerate the CaO solids and produce a rich CO_2 stream ready to be compressed and transported for storage or other uses.

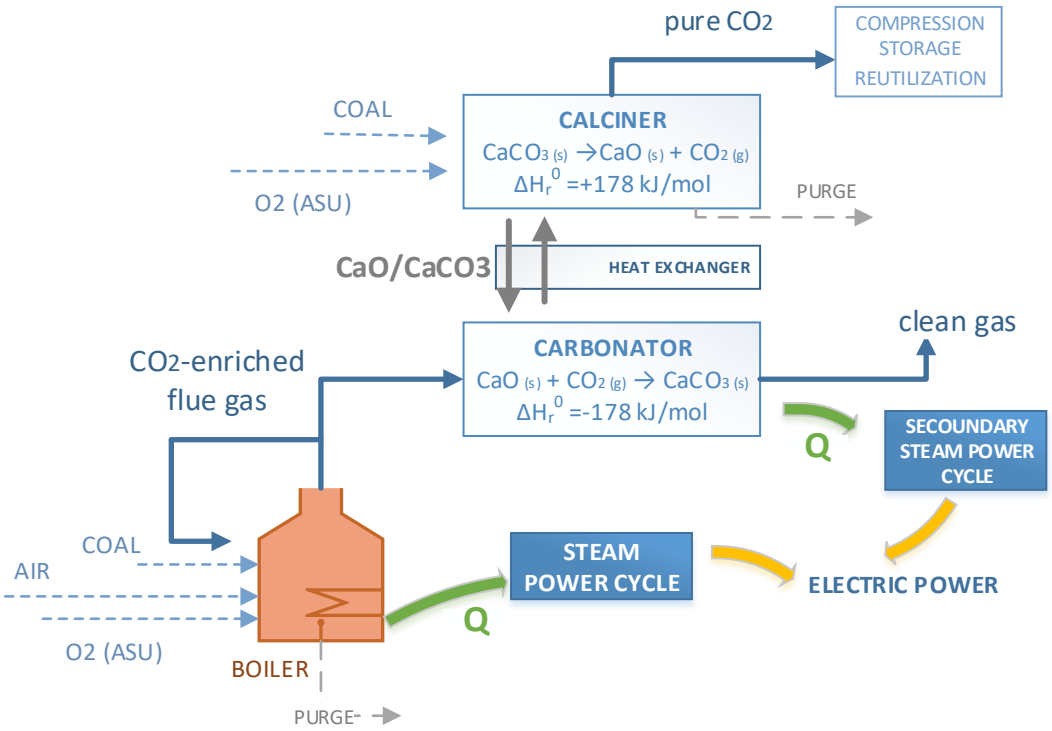

Figure 4: Oxy-CaL process schematics

b. CO_2 capture efficiency (carbonator model)

The CO_2 capture efficiency in the CaL process will be analyses by means of the carbonator model described in detail elsewhere [38]. Accordingly, the CO_2 capture efficiency can be expressed as a function of the total solids inventory in the carbonator (W_s), or the moles number of Ca-based solids (N_{Ca}), the CaO/$CaCO_3$ particles residence time in the carbonator (τ) and the makeup flow of fresh limestone fed into the system (F_0). In this model an average CaO conversion (X_{ave}) is defined by the sum of the average conversion in the fast reaction-controlled phase ($X_{ave,FRP}$) and conversion in the solid-state diffusion controlled phase ($X_{ave,SDP}$), where both $X_{ave,FRP}$ and $X_{ave,SDP}$ are calculated by assuming that the gas passes in plug flow across a bed of perfectly mixed solids in the carbonator. The interested reader may see the work of Ortiz et al. [38] for further details on the carbonator model.

According to this carbonator model, the average reaction rates in the FRP and SDP phases are expressed as:

$$r_{ave_{FRP}} = \frac{X_{ave_{FRP}}}{t_{FRP}} \quad for \quad t \le t_{FRP} \qquad (2)$$

$$r_{ave_{SDP}} = \frac{X_{ave_{SDP}}}{t_0 - t_{FRP}} \quad for \quad t_{FRP} < t \le t_{max} \qquad (3)$$

where $r_{ave,_i}$ is the average reaction rate in the i-phase (either FRP or SDP), t_{FRP} is the time lag of the FRP phase, t_{max} is total carbonation time, $X_{\mathrm{ave,i}}$ is the average capture capacity in the i-phase, and t_0 is the overall carbonation time lag in the carbonation TGA test (section 2).

The average rate of CaO conversion in the kinetically controlled fast phase ($r_{ave_{FRP}}$) at atmospheric pressure can be approximated by a first-order kinetic law [30]:

$$r_{ave_{FRP}} = k_s S_{ave}(1 - X)^{\frac{2}{3}}\left([CO_2] - [CO_2]_{eq}\right) \quad (4)$$

where $[CO_2]$ and $[CO_2]_{eq}$ are the actual and equilibrium CO_2 concentrations, respectively, k_s is the kinetic constant and S_{ave} is the average CaO specific surface area available for reaction after N cycles.

On the other hand, the average rate of CaO conversion in the diffusion controlled phase can be expressed by means of an effective diffusion constant ($D^*{}_{eff}$) [38].

$$r_{ave_{SDP}} \approx D^*{}_{eff}\left([CO_2] - [CO_2]_{eq}\right) \quad (5)$$

Both Eq.4 and Eq.5 can be well fitted to the experimental TGA data shown above, which allows us obtaining the values of k_s and $D^*{}_{eff}$ to be used in the kinetic model for each one of the CaL and oxy-CaL systems considered. Values of best fitting parameters are shown in Table 2.

Table 2: Kinetic model parameters obtained from the best fits of Eqs. 4 and 5 to experimental TGA data.

	$k_s(\text{x } 10^{10})\left[\frac{\text{m}^4}{\text{mol}\cdot\text{s}}\right]$	$D^*{}_{eff}$ (x 10^5) $[\frac{\text{m}^3}{\text{mol}\cdot\text{s}}]$
CaL-625	8.87	2.70
CaL-650	10.00	4.63
CaL-680	12.27	8.09
Oxy-CaL30-625	4.429	1.07
Oxy-CaL30-650	6.08	1.61
Oxy-CaL30-680	4.51	2.75
Oxy-CaL45-625	3.21	0.61
Oxy-CaL45-650	3.60	1.02
Oxy-CaL45-680	2.75	1.68
Oxy-CaL60-625	2.00	0.61
Oxy-CaL60-650	2.38	0.71
Oxy-CaL60-680	1.98	1.10

Once the average CaO conversion is calculated, the capture efficiency in the carbonator (E_{CO2}) can be obtained as:

$$E_{CO2} = \frac{F_R}{F_{CO2}} X_{ave} \qquad (6)$$

where F_R is the solids recirculation flow rate between the carbonator and calciner reactors, which is given by $F_R = W_s/N_{Ca}$.

Figure 5 shows the evolution of the CO_2 capture efficiency (E_{CO2}) as the solids recirculation flow rate between reactors is decreased or, equivalently, the solids residence time in the carbonator ($\tau = N_{Ca}/F_R$) is increased. As may be seen, a significantly higher capture efficiency is achieved by increasing the CO_2 concentration in the carbonator in the Oxy-CaL systems. Note the differences on the maximum capture efficiency ($E_{max} = (y_{CO2,in} - y_{eq})/y_{CO2,in}$)) for the different systems (obtained for very short residence times) as a consequence of the variation of the CO_2 vol % in the carbonator. Even though the use of short residence times leads to relatively high capture efficiencies it must be kept in mind that short residence times would rise the cost for solids transportation. The sensible heat needed to increase the temperature of the solids stream entering the calciner would be also raised as the solids recirculation rate is increased to achieve short residence times.

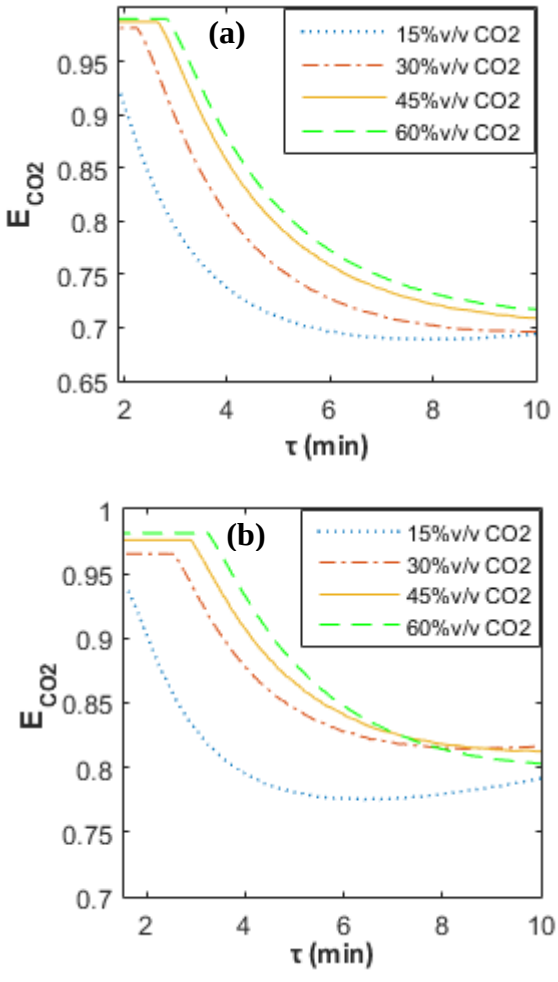

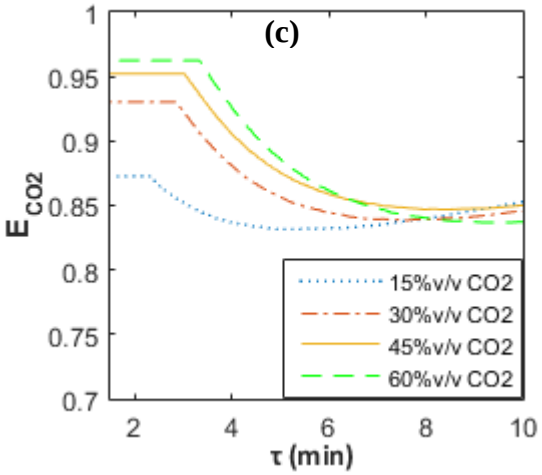

Figure 5: CO_2 capture efficiency as a function of the residence time in the carbonator, which is varied by changing the F_R/F_{CO2} ratio. Calculations are made for fixed values of the solids inventory $W_s = 400\ ton$ and $F_0/F_{CO2} = 0.05$ and different carbonation temperatures. a) $T_{carb} = 625ºC$; b) $T_{carb} = 650ºC$ and c) $T_{carb} = 680ºC$.

A shown in Figure 5, the capture efficiency is decreased as the solids residence time in the carbonator is prolonged albeit at a minor rate for the CaL process in comparison with the Oxy-CaL systems. This is due to the relatively higher conversion in the solid-state diffusion controlled phase for the CaL process (as seen above from the TGA tests). This result becomes more marked as the carbonator temperature is increased (compare Figure 5a and Figure 5c) as a consequence of the enhancement of solid-state diffusivity with temperature. The results obtained up to this point show already some hints concerning the CFPP-CO_2 capture integration. An increase in the solids residence time in the carbonator would arguably allow for a reduction of the energy penalty although the capture efficiency would be hampered depending on the capture system. Thus, a comparative assessment of the diverse capture systems and their integration into CFFP must necessarily include an evaluation of the energy penalty. This will be the subject of the next section.

4. CFPP-CO_2 capture integration models

This section is devoted to a comparative assessment of several CO_2 capture technologies, namely oxy-combustion, CaL and Oxy-CaL, and their integration into a Coal Fired Power Plant (CFPP). Regarding energy penalty, the parameter usually employed in the literature is the specific energy consumption for CO_2 avoided (SPECCA) [7], which quantifies the additional fuel consumption (in MJ) needed to avoid the emission of 1 kg of CO_2 into the atmosphere (Eq.6).

$$\text{SPECCA}\ [MJ/kg_{CO_2}] = 3600\ \frac{\frac{1}{\eta_{plant}} - \frac{1}{\eta_{ref}}}{E_{ref} - E} \qquad (6)$$

where η_{ref} , η_{plant} are the CFPP efficiency, and E_{ref}, E are the emissions ratio (in kg CO_2/kWh$_e$) without and with the capture system integrated, respectively.

A 490 MW_e CFPP has been chosen in our work as reference plant, which is modelled using the commercial software ASPEN PLUS™. The main model assumptions are summarized as follows: (i) the system operates at steady conditions; (ii) minimum temperature difference is 20ºC for all heat exchangers; (iii) ideal behavior of cyclones; (iv) solid–solid heat exchange is simulated as a transfer of heat between solids; (v) 89% isentropic efficiencies are assumed as constant for all turbomachinery. In this CFPP, air-combustion of 42.2 kg/s of coal Pittsburgh No. 8 (see [39] for coal type details) takes place in the steam boiler (operating at an average temperature of 900ºC) to generate 1297 MW_{th}, which releases to the atmosphere 513.4 kg/s of flue gas with a CO_2 vol concentration of 15% at atmospheric pressure. Electric power is produced by means of a reheat supercritical steam cycle (P_{vv} = 290 bar, T_{vv} = 600/620ºC), wherein the steam regenerative process is carried out from four feed-water heaters, one of which is a total mixer exchanger type (degasifier). Selected conditions lead to a 44% thermal to electric net efficiency. Taking into account parasitic electricity, the overall net efficiency drops to 37.77%. This value will be used as a reference to calculate the penalty arising from the integration in this plant of the diverse CO_2 capture systems. Main inputs and results from the reference plant model are summarized in Table 3. An extended table showing additional parameters is shown in Appendix B. Table 3 shows main inputs and derived outputs for the three cases analyzed in this section: oxy-combustion (case a), calcium looping (case b) and hybrid combination of both (case c) with different values of CO_2 in vol% . They are described in detail following in this section.

Table 3: Main inputs and results for the base case of diverse CO_2 capture systems

	parameter	Reference CFFP (air combustion)	Case a	Case b	Case c		
			oxy-combustion	CaL	Oxy-CaL 30	Oxy-CaL 45	Oxy-CaL 60
CFPP	$\dot{m}_{coal}\ (kg/s)$	42.20	55.05	42.20	46.10	47.50	48.15
	$\dot{m}_{air}\ (kg/s)$	475	-	475	208.90	100.20	43.54
	$\dot{m}_{O2}\ (kg/s)$	-	136.91	-	68.85	96.35	110.503
	v_{CO2}	0.15	0.89	0.15	0.30	0.45	0.60
	η_{CFPP}	0.3777	0.2872	0.3777	0.3517	0.3437	0.3374
	$net\ work\ (MW)$	490.47	488.80	490.47	498.30	502.30	499.75
	$Penalty$	-	**9.05%**	-	**2.60%**	**3.40%**	**4.03%**
	$SPECCA$ (MJ/kg_{CO2})	-	**4.06**	-	**0.94**	**1.25**	**1.50**
CaL	$T_{calc}\ (ºC)$	-	-	950	950	950	950
	$T_{carb}\ (ºC)$	-	-	650	650	650	650
	E_{CO2}	-		0.827	0.950	0.976	0.981
	$\dot{m}_{coal}\ (kg/s)$	-	-	18.48	22.34	23.40	23.84
	$\dot{m}_{O2}\ (kg/s)$	-	-	48.00	58.41	61.00	62.49
	$\dot{W}_{sec}\ (MW)$	-	-	75.80	113.90	126.46	130.88
	η_{int}	-	-	0.3030	0.2909	0.2882	0.2853
	$Penalty$	-	-	**7.47%**	**6.08%**	**5.55%**	**5.21%**
	$SPECCA$ (MJ/kg_{CO2})	-	-	**3.28**	**2.63**	**2.37**	**2.29**
Total	$\dot{m}_{coal,total}$	-	-	60.68	68.44	70.90	71.99

	$Penalty_{total}$	-	**9.05%**	**7.47%**	**8.68%**	**8.95%**	**9.24%**
	$SPECCA_{total}$ (MJ/kg_{CO2})	-	**4.06**	**3.28**	**3.56**	**3.62**	**3.79**

a. Total Oxy-combustion

Firstly, an oxy-fuel combustion process will be analyzed in order to assess the CO_2 capture efficiency and the energy consumption in comparison with the above-mentioned reference plant. The CFPP oxy-combustion model has been developed using ASPEN PLUS™ and the same coal (Pittsburgh No. 8). Figure 6 shows a flow diagram of the oxy-combustion model that highlights the differences with respect to the reference air-combustion plant. For simulating coal oxy-combustion a reactor model based on Gibbs' free energy minimization method is used.

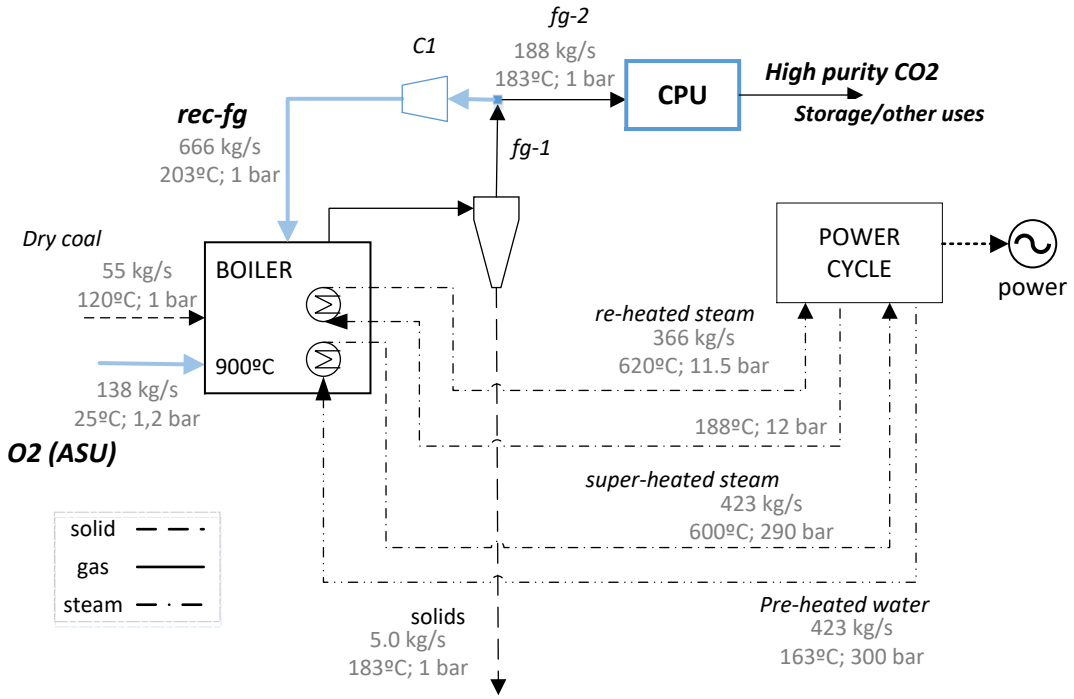

Figure 6: Schematics of the total oxy-combustion CFPP. Differences with air-combustion CFPP are highlighted in blue color (for interpretation of the references to color in this figure, the reader is referred to the web version of this article.)

In this CFPP oxy-combustion case, combustion of 55.3 kg/s of coal Pittsburgh No. 8 with 137.6 kg/s of a high purity (95%) O_2 stream from ASU releases 187.8 kg/s of flue gas with a CO_2 vol concentration (dry-basis) of 89% at atmospheric pressure, which, after purification and compression, is ready to be stored [40] or used in other industrial processes [41,42]. A flue gas recirculation with a recycle ratio of 0.78 is carried out in order to control the flame temperature in the boiler [43]. A compressor (C1 in the figure) is used to overcome the pressure drop in the reactor. ASU energy consumption has been estimated as 200 kWh per kg of pure O_2 [44,45]. CO_2 purification unit (CPU) specific energy consumption has been fixed to 143 kWh/tCO_2 [22] in order to simplify the model. Power is produced using the same reheat supercritical steam cycle (P_{vv} = 290 bar, T_{vv} = 600/620ºC) as in the reference air-combustion CFPP case. Main

inputs and results from the model are summarized in Table 3. From the simulations, the resulting specific CO_2 emissions are 86.2 g/kWh corresponding to 90% CO_2 capture efficiency. Remaining CO_2 emissions result from the nearly 8% of CO_2 lost in the purification process, which is consistent with results from previous works [40]. A net thermal to electric efficiency of 28.8% is achieved yielding an energy penalty of 9.1% points, which is within the range of previously reported results (8-12%) [18,46].

b. Calcium-Looping

In this section, the CaL integration model for post-combustion CO_2 capture used in the present work is summarized. The reader interested in further details may see the work of Ortiz et al. [47] where a similar model is thoroughly described. The CaL process is accomplished by using two interconnected circulating- fluidized-bed (CFB) reactors, both operated under atmospheric pressure at gas velocities of approximately 5 m/s [48,49]. CaO particles react in the carbonator according to the carbonation reaction (Eq.7) at temperatures between 625-680ºC with the CO_2 present in the flue gas stream coming from the CFPP plant. The partially carbonated particles are then circulated into the calciner reactor in which fast decomposition of $CaCO_3$ occurs at 950ºC [15,25,50,51] to regenerate the sorbent and produce a rich CO_2 stream to be compressed and transported for storage or other uses. At calciner exit, CaO particles are recovered by a cyclone and sent back to the carbonator for a new cycle. CO_2 capture in this reactor is modeled according to an equilibrium reactor following the model described in section 3.b:

$$CaO + CO_2 \rightleftarrows CaCO_3 \qquad \Delta H_r^0 = -178\frac{kJ}{mol} \qquad (7)$$

Figure 7 shows a schematic representation of the CaL process. Steam is used as heat carrier fluid to take advantage of heat produced in the exothermic carbonation reaction for electricity generation by means of a secondary steam cycle. Moreover, the sensible heat from the CO_2 stream exiting the calciner is also used to increase the steam production. Since a large flow rate of solids are recirculated in the CaL cycle, a heat exchanger (simplified as a heat transfer between solids with a temperature approach of 20ºC) is incorporated for transferring sensible heat between the CaO particles leaving the calciner (F_R in Figure 7, with a temperature of about 950ºC) and the solids (CaCO3 and unreacted CaO particles) entering into it to be heated up to the calcination temperature.

In order to attain full calcination in short residence times of the limestone makeup fed into the calciner, the temperature in the calciner reactor must be 930º o even higher [14,52]. This makes necessary to supply a large amount of heat to the calciner, which is accomplished by in-situ oxy-fuel combustion in order not to dilute CO_2 in this reactor. CO_2 compression is modelled as a multi-stage compression to 100 bar refrigerated with water from the low-pressure section of the steam cycle. Pressure drop of the flue gas across the carbonator is calculated from the Kunii–Levenspiel (K–L) fluid dynamics model [53,54]. A compressor is used to counteract this pressure drop. Energy consumption derived from solids transportation has been set at 20 MJ per ton of solids [55]. Main inputs and results from the model are summarized in Table 3. The

base case for CFPP-CaL integration leads to a CO_2 capture efficiency of 82.7% for an overall plant efficiency of 30.3%, which implies an energy penalty of 7.4% points in the range of previous values reported in literature [6,56,57]. As regards specific energy consumption (Eq. 6), a SPECCA value of 3.3 MJ/kg CO_2 is achieved.

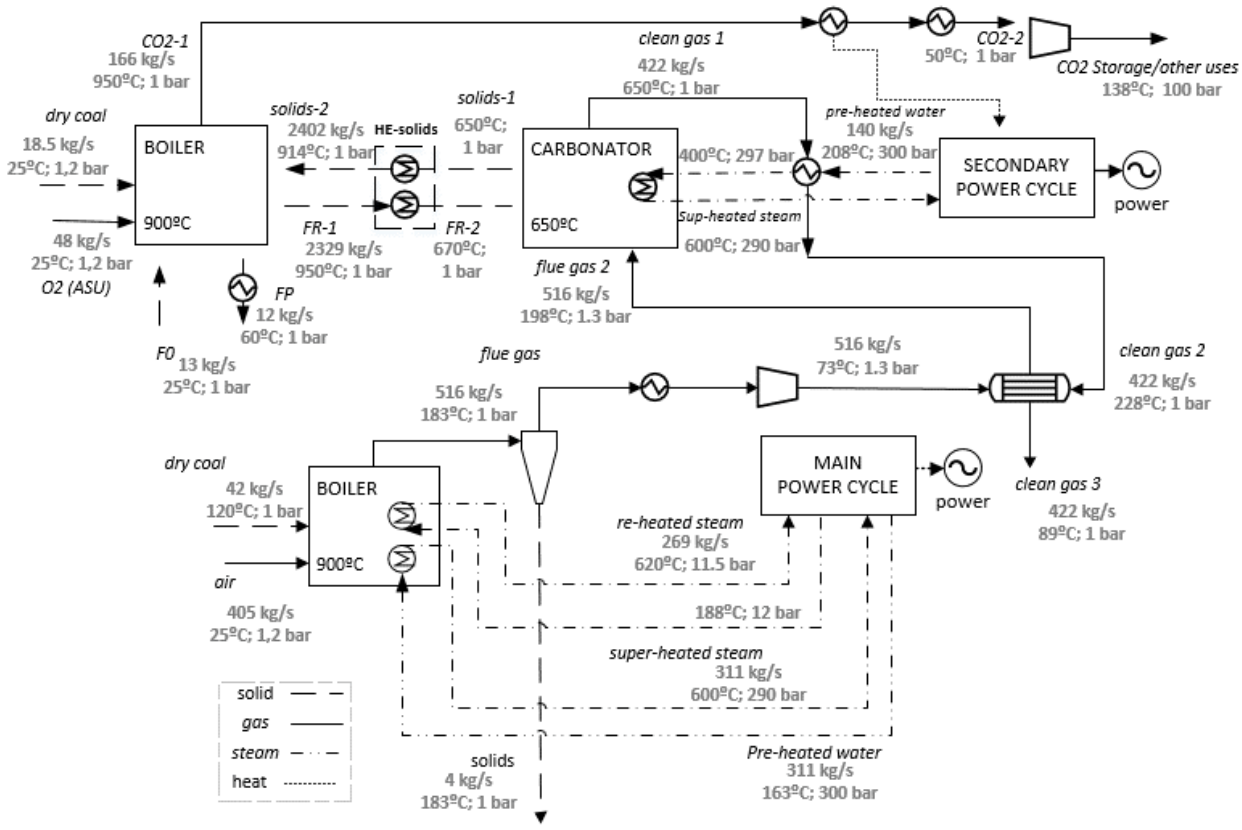

Figure 7: CFPP-CaL integration scheme

c. Oxy-CaL

This section describes the novel Oxy-CaL hybrid system proposed in the present work. Figure 8 shows a schematic representation of the process, which has been simulated for several values of the CO_2 vol % in the flue gas effluent from partial oxy-combustion. As can be seen in Figure 8, the process is initiated by an oxy-fuel combustion similar to that described in section 4.a. Partial oxy-combustion is carried out to obtain a CO_2 vol% in the range of 30-60% in the flue gas at the boiler exit. To this end, a mixture of air and O_2 is used in the boiler for combustion. The air/O_2 ratio is calculated to achieve a given CO_2 vol% in the flue gas (45% in the case illustrated in Figure 8). As in the case of total oxy-combustion, recirculation of the flue gas serves to control the flame temperature in the boiler, whose value is kept the same for all the simulations.

Since the amount of pure O_2 for partial oxy-combustion is substantially decreased (99.3 kg/s to achieve a 45% vol CO_2 concentration instead of 138 kg/s for total oxy-combustion), power

consumption in the ASU is notably reduced. Furthermore, the CPU unit for CO_2 purification is not needed since this step is carried out after the CaL process. Altogether, the energy penalty for partial oxy-combustion is significantly reduced. Thus, energy penalty is 3.40% in the Oxy-CaL 45 system as compared to 9.05% for total oxy-combustion.

After partial oxy-combustion, the CO_2 rich flue gas is sent to the carbonator reactor to follow up with the CaL process, being before slightly compressed (to overcome the pressure drop in the carbonator) and preheated with the hot gas streams exiting the CaL cycle. In contrast with the CaL scheme (Figure 7), flue gas preheating is carried out in the Oxy-CaL system by using firstly the compressed CO_2 stream since the thermal capacity of the flue gas at the carbonator exit is lower than in the case of the CaL. The CO_2 entering into the carbonator reacts with the CaO solids coming from the calciner as in the conventional CaL model (section 4.b) according to the carbonation reaction (Eq. 7). As discussed in section 3, the capture efficiency is significantly enhanced when the CO_2 concentration in the flue gas is increased (Figure 5). Thus, the Oxy-CaL-45 system has a CO_2 capture efficiency of 97.6% in the base case (see Figure 5a) as compared to 82.7% in the base case of the CaL system. Such increase in the capture capacity implies also the handling of a larger amount of $CaCO_3$, which leads to higher heat needs in the calciner for CaO regeneration, and therefore to a higher consumption of coal and O_2 as can be seen by comparison of Figure 7-9. Nonetheless, the amount of CO_2 captured in this Oxy-CaL-45 system is 29% over that captured by means of CaL (section 4.b) and 14% above the CO_2 captured by total oxy-combustion (section 0).

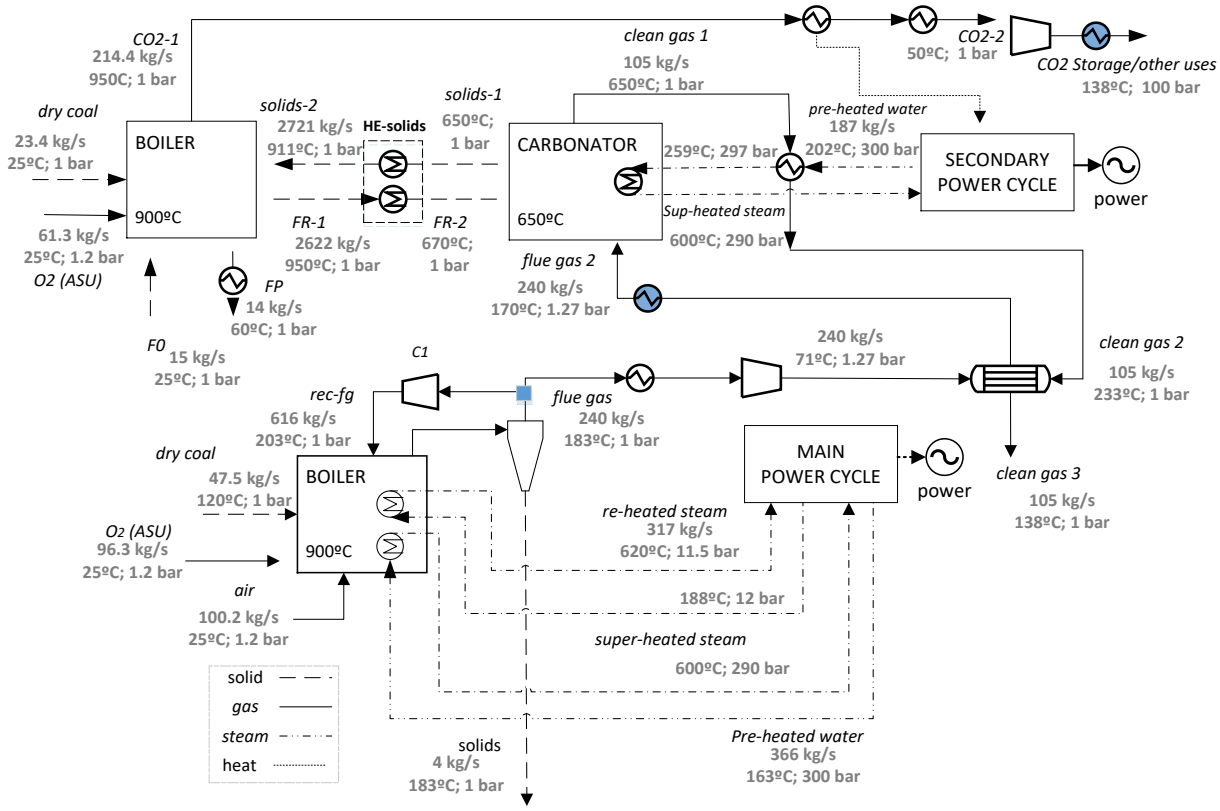

Figure 8: General Oxy-CaL-45 (45% vol CO_2 concentration in the flue gas by partial oxy-combustion) integration scheme

Despite the need of additional coal and O_2 for oxy-combustion in the calciner, the increase in CO_2 capture efficiency obtained by increasing the CO_2 concentration in the flue gas leads to a reduction of energy consumption in the CaL cycle. Thus, a SPECCA value of 2.37 MJ/kg CO_2 is obtained for the Oxy-CaL-45 system, which is 28% below the SPECCA obtained for the conventional CaL system. Nevertheless, the SPECCA for the complete oxy-CaL process is 3.62 MJ/kg CO_2, which is 10% higher than in the CaL base case. On the other hand, the Oxy-CaL system allows for a reduction by 11% of energy consumption in comparison with the total oxy-combustion case. The next sections are devoted to a deeper comparative analysis on both capture efficiency and energy penalty resulting from the diverse capture systems with the goal of finding the most feasible choice to be implemented in practice.

5. CO_2 capture efficiency and energy consumption

As was shown in sections 2.b (TGA results) and 3.b (carbonator model), the CO_2 capture efficiency in the CaL process is remarkably enhanced by increasing the CO_2 concentration in the flue gas stream entering into the carbonator. This is reflected also in the SPECCA, which is decreased due to the higher efficiency of the CO_2 capture process. On the other hand, partial oxy-combustion carried out to increase the CO_2 concentration at the inlet of the carbonator in the CaL process contributes also to an additional energy penalty. The use of the CaL process, total oxy-combustion or a hybrid Oxy-CaL process for CO_2 capture in CFPP is carefully assessed below on the basis of the benefits and drawbacks of each one of these systems.

Figure 9 shows the CO_2 capture efficiency and SPECCA values for total oxy-combustion, CaL, and Oxy-CaL systems obtained for the base cases analyzed in section 4. As seen in Figure 9a, the part of SPECCA that corresponds to the CaL process in the Oxy-CaL systems is decreased as the carbonation CO_2 vol% is increased if the oxy-CaL process is operated with a high solids recirculation flow rate (F_R/F_0=15 corresponding to τ =2 min for the solids residence time and fixing Ws=400 tons as solids inventory). Nevertheless, energy consumption in the partial oxy-combustion part of the process leads to global oxy-CaL SPECCA values somewhat higher than for the purely CaL process. On the other hand, the oxy-CaL 30 , 45 and 60 systems have a SPECCA smaller than total oxy-combustion. Note also that the CO_2 capture efficiency is notably increased for the oxy-CaL systems as compared to oxy-combustion and is especially increased over the CaL process. Figure 9b shows however that under prolonged solids residence times of τ =10 min (corresponding to a reduced solids recirculation flow F_R/F_0=4 and fixing Ws=400 tons as solids inventory) the capture efficiency of the oxy-CaL systems is hindered since carbonation in the solid-state diffusion controlled stage is not significant for carbonation under relatively high CO_2 vol% as was seen from the TGA tests (section 3.b).

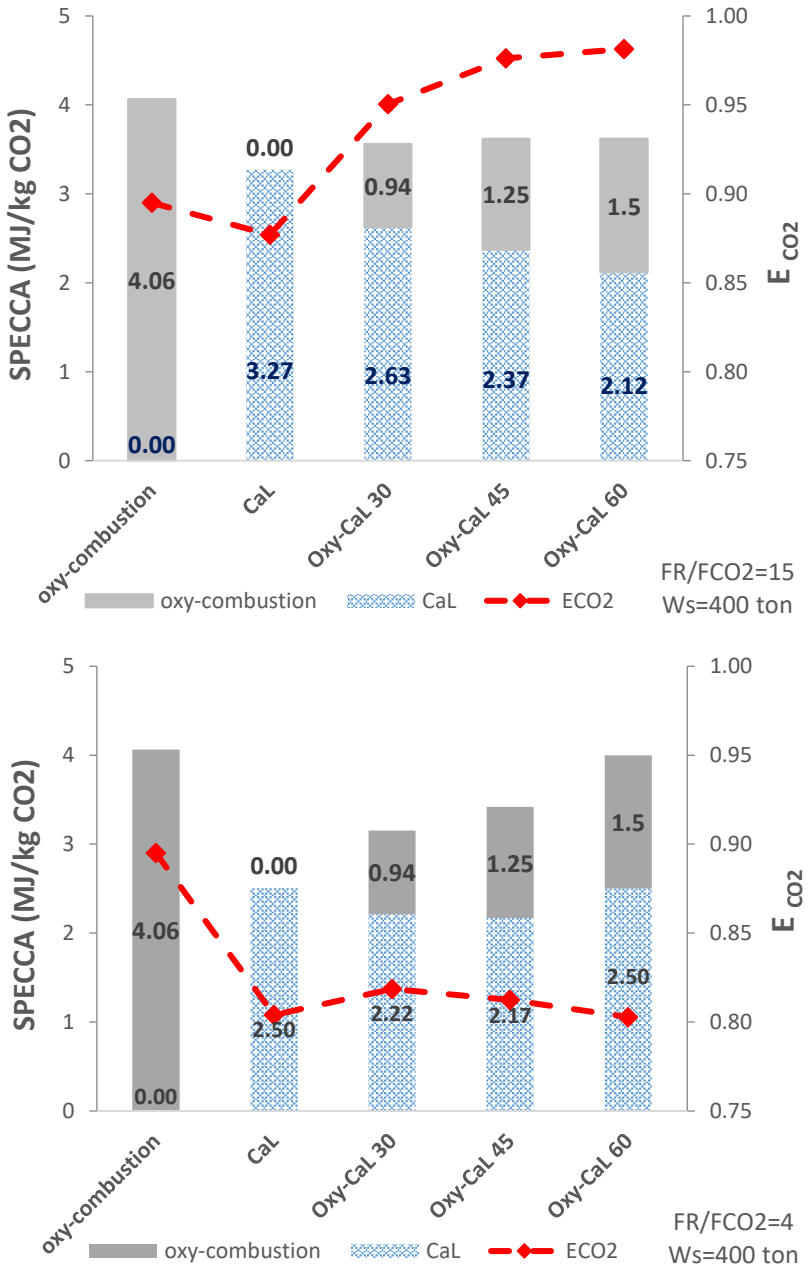

Figure 9: SPECCA values and CO_2 capture efficiencies for the CO_2 capture systems analysed in this work and using reference parameters shown in table 3. Figures a) and b) correspond to different values of the solids residence time τ in the carbonator for the CaL process. a) FR/FCO_2=15 (τ=2 min), b) FR/FCO_2=4 (τ =10 min).

As discussed above and according to recent works [13,47], energy consumption in the CaL process is highly dependent on the carbonation rate in the solid-state diffusion controlled phase (SDP), which determines the role of the solids residence time τ in the carbonator. Figure 10 shows how SPECCA evolves as τ is increased for the CaL and hybrid oxy-CaL processes. In the case of the CaL process, the rate of carbonation in the solid-state diffusion controlled phase is not negligible as compared to the carbonation rate in the fast reaction controlled phase, which leads to a considerable reduction of the energy consumption as τ is increased [13,47]. On the other hand, the rate of carbonation in the solid-state diffusion controlled phase is decreased by

increasing the CO_2 concentration in the flue gas as occurs in the oxy-CaL systems (see Figure 1), which hinders a further reduction of SPECCA as τ is increased. For the Oxy-CaL-60 case, the SPECCA is even raised as τ is prolonged beyond ~4 min. On the other hand, the SPECCA values for the CaL and oxy-CaL systems are similar for short solids residence time (of about 2 minutes). Thus, it may be concluded that the optimum operation of the oxy-CaL system is under short residence times.

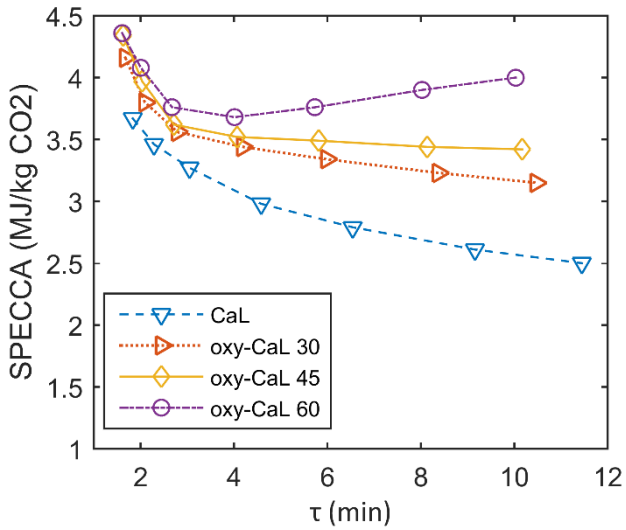

Figure 10: SPECCA values as a function of solids residence time in the carbonator for CaL and Oxy-CaL systems operating at T_{carb}=650ºC (solids inventory fixed at Ws=400 ton).

5.1 Role of solids inventory

A straightforward consequence of the improvement of CO_2 capture efficiency in the CaL process as the CO_2 vol% in the carbonator is increased (Oxy-CaL) is the possibility of reducing the solids inventory (W_s) and the limestone makeup flow (F_0), which could lead to a potentially relevant capital and operational cost cutback. Figure 12a shows the variation of the solids inventory (W_s) in the CaL and oxy-CaL processes with the solids residence time for a fixed value of the capture efficiency (E_{CO2}= 90%). As can be seen, significantly lower solids inventories are needed in the Oxy-CaL processes under carbonation residence times below ~12 minutes that would conform to usual operation conditions in CFB reactors. This result implies an important potential for reducing the CaL size in the hybrid oxy-CaL systems. It must be reminded that system size is currently one of the main limitations for the CaL process to reach a demonstration stage [4,16]. Moreover, a lower solids inventory, as would be possible in the Oxy-CaL system, leads to a reduction of power consumption to overcome the gas pressure drop across the reactor. The oxygen production and coal input needed for heating-up the additional quantity of solids in calciner are also diminished.

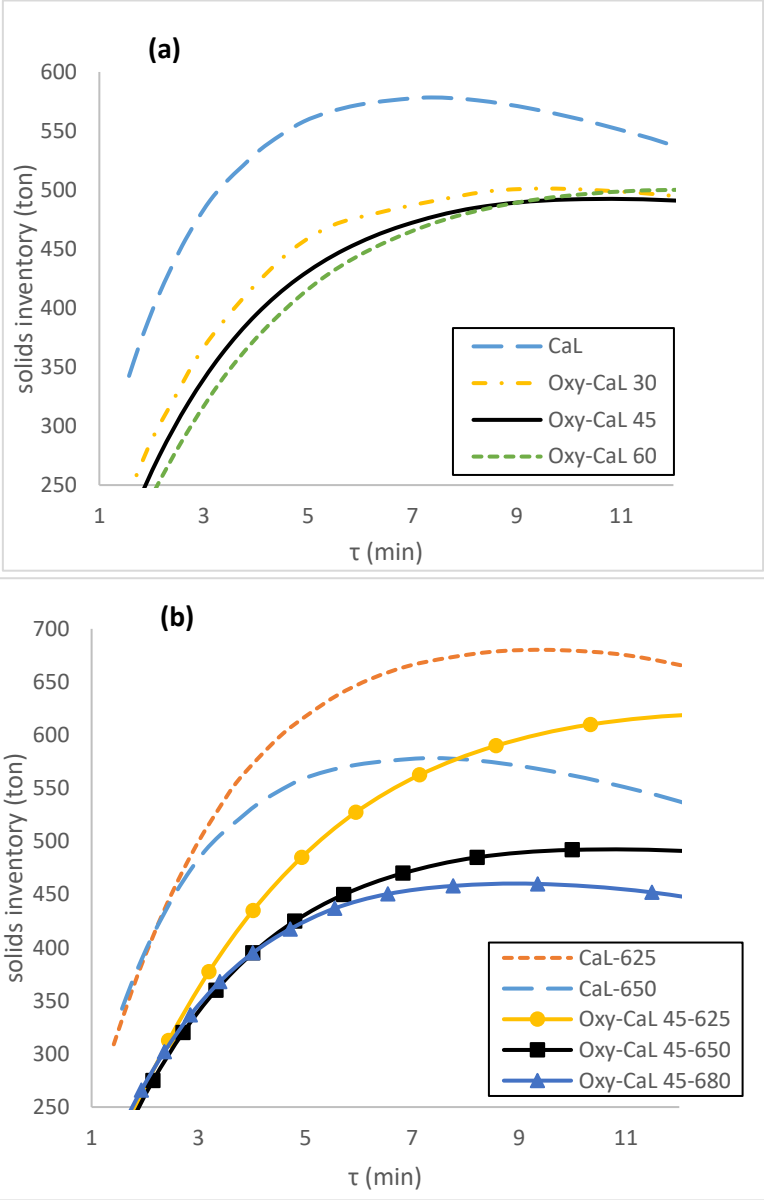

Figure 11: 90% capture iso-efficiency lines as a function of solids inventory and solids residence time in the carbonator for CaL and Oxy-CaL systems at a carbonator temperature Tcarb=650ºC (a) and for the CaL and Oxy-CaL-45 systems at carbonation temperatures of 625, 650, and 680ºC (b).

Figure 11b shows the evolution of W_s with the solids residence time in the carbonator for carbonation temperatures T=625ºC, 650ºC and 680ºC and a fixed capture efficiency (E_{CO2}= 90%). As may be observed, the relative decrease of the carbonation rate in the solid-state diffusion controlled stage when T is decreased to 625ºC leads to a remarkable increase of W_s for solids residence times beyond ~3 min. Thus, the CaL process operated under long residence times, which would allow decreasing notably SPECCA [13,47], can be hampered by a small decrease of the carbonator temperature that might be expected locally under practical conditions [14,48] due to inefficient mass and/or energy transfer. Note that chemical equilibrium prevents in the case of the CaL process to achieve a 90% capture efficiency when operating at 680ºC (see the maximum capture value possible in Figure 5a). On the other hand, since the Oxy-CaL

system would be ideally operated under short residence times, its performance would not be essentially affected by temperature changes.

As seen in the results obtained from our TGA experiments (Figure 2), the rate of carbonation in the solid-state diffusion controlled phase depends critically on the carbonator temperature. Thus, carbonation in this phase is hindered if the temperature is decreased just from 650ºC to 625ºC whereas it becomes enhanced by an increase of temperature up to 680ºC. It is therefore interesting to assess the sensitivity of SPECCA and solids inventory needed in the CaL process to this small change of carbonation temperature that might occur in practice.

Despite the potential for reducing the CaL size in the Oxy-CaL process, the additional energy consumption due to partial oxy-combustion, and therefore O&M costs, must be also considered to assess the Oxy-CaL feasibility. In this regard, a further benefit of the Oxy-CaL hybrid system is that the higher capture efficiency achieved allows to reduce the fresh limestone fresh makeup, which yields a decrease of energy penalty. Figure 12 shows the relationship between the solids inventory and make-up flow for the diverse systems analyzed at a fixed capture efficiency of 90%.

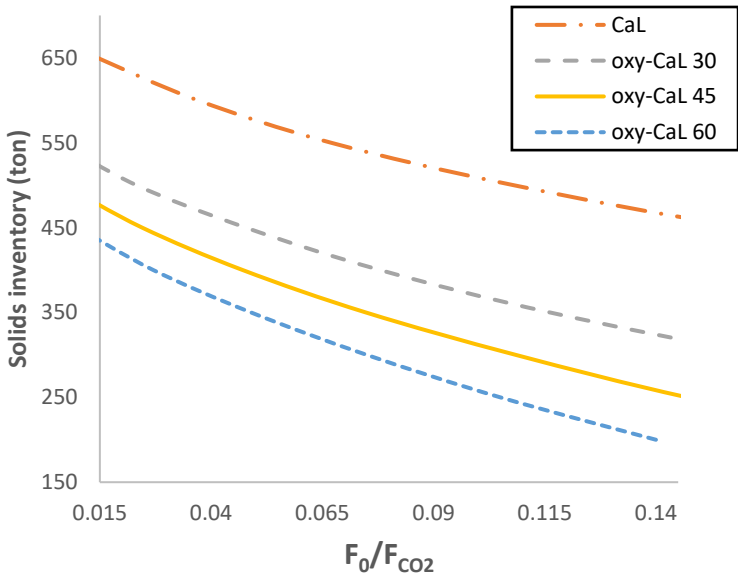

Figure 12: Solids inventory as a function of makeup flow for CaL and Oxy-CaL systems at a carbonator temperature Tcarb=650ºC and at capture efficiency of 90%. Solids recirculation flow rate is fixed to F_R/F_{CO2}=15.

As can be seen in Figure 12, by using the Oxy-CaL hybrid system it is possible to reduce considerably the fresh limestone makeup in comparison with the CaL process. For example, if we consider the Oxy-CaL 45 system with a solids inventory of 450 tons, the ratio of limestone makeup to CO_2 flow rates (F_0/F_{CO2}) is just around 0.015, which is quite below the amount needed for the CaL process under the same operation conditions and capture efficiency (F_0/F_{CO2}=0.12). Figure 13 shows the SPECCA values obtained by fixing the solids inventory at 450 tons and varying the makeup flow to attain with each system a capture efficiency of 90%.

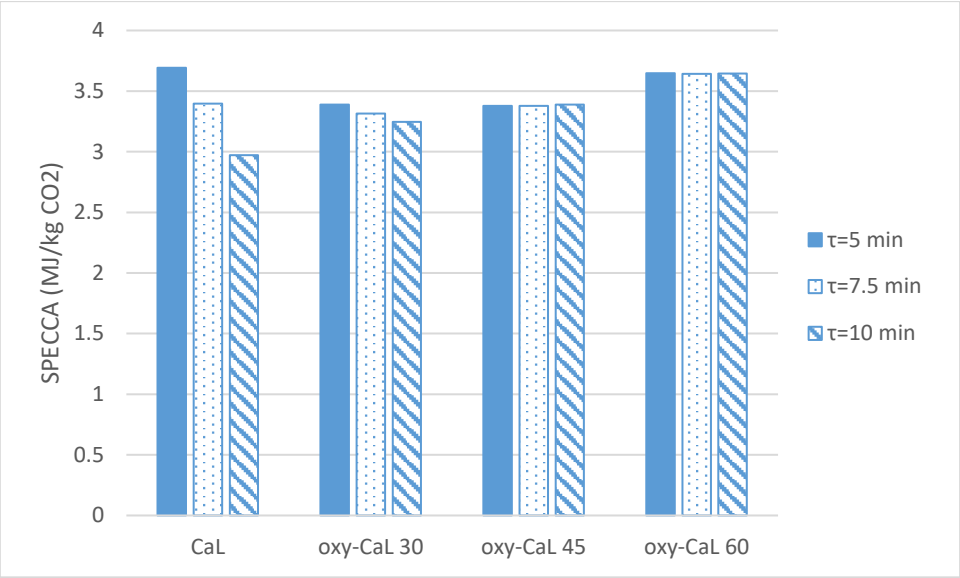

Figure 13: SPECCA values for the CaL and Oxy-CaL systems obtained by considering a fixed solids inventory of Ws=450 tons and capture efficiency to 90%.

As shown in Figure 13, using a given solids inventory of 450 tons in the carbonator, SPECCA values for Oxy-CaL systems are lower than for the CaL process when operating under solids residence times below 7.5 min due to the lower makeup flow needed to reach a 90% capture efficiency. Thus, the use of the Oxy-CaL systems would allow also for a reduction of O&M costs associated to the capture process using typical reactor sizes. On the other hand, if the solids residence time is prolonged to 10 min, the CaL process yields a lower SPECCA due to promoted carbonation in the solid-state diffusion controlled phase.

Figure 14 shows data on SPECCA and solids inventory for the CaL and Oxy-CaL (carbonator temperatures of 625ºC, 650ºC and 680ºC) systems for a fixed capture efficiency (E_{CO2}= 90%), and short (2 min) and prolonged (10 min) solids residence times. A may be seen, for operation under short residence times, the Oxy-CaL systems (especially Oxy-CaL-30 and 45) lead to a considerable reduction of the solids inventory (from 400 tons for the CaL-650 system to 286 tons for Oxy-CaL-45-650) and therefore to a reduction of the CaL system size whereas the SPECCA is only slightly increased (from 3.59 MJ/kg for the CaL-650 system to 3.7 MJ/kg for the Oxy-CaL-45-650). Regarding the effect of carbonator temperature on the CaL and Oxy-Cal systems for a given solids residence time of 2 min, there is not a clear evidence on the optimum system choice (lower SPECCA). On the other hand, for longer residence times (Figure 14b), the CaL-625 system shows a better performance in terms of efficiency albeit a considerable higher solids inventory is required in this case. Thus, the CaL process advantage is lost by a modest decrease of the carbonator temperature, which would require a considerable increase of the solids inventory to ensure a high capture efficiency. At this point, it is important to note that both CaL and Oxy-CaL systems yield a lower energy consumption than the conventional oxy-fuel combustion process regardless of the carbonator temperature and carbonator CO_2 concentration.

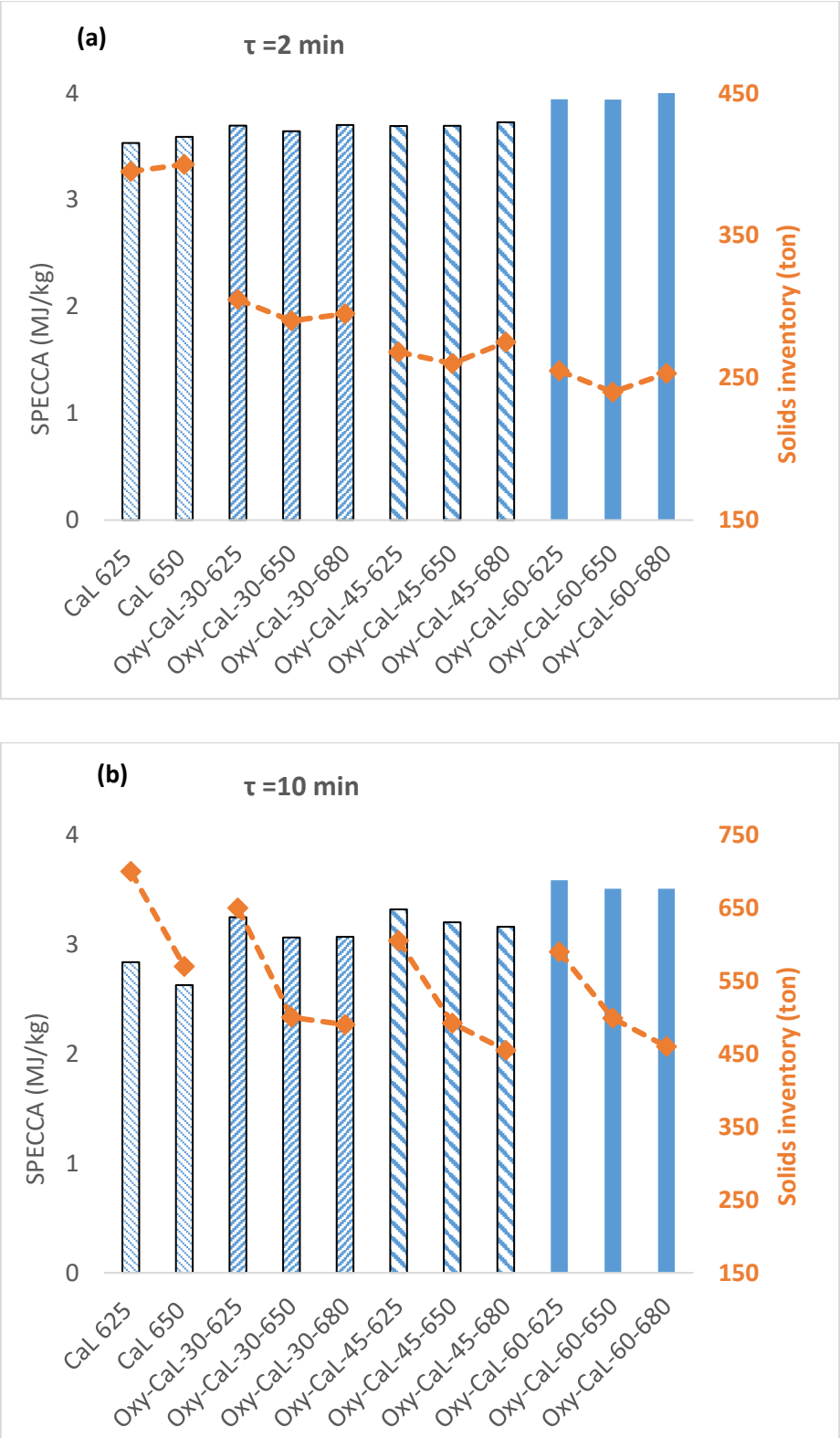

Figure 14: SPECCA and solids inventory for the CaL and Oxy-CaL systems operating under a) short (2 min) and b) prolonged (10 min) solids residence times. The effect of changing the carbonator temperature (between 625ºC to 680ºC) is also shown. Capture efficiency is fixed to 90%.

Concerning the Oxy-CaL-30 system operated under short residence times, it would allow reducing the solids inventory from 400 tons (CaL-625) system to 300 tons (-33% relative

reduction) and thus the reactors (carbonator and calciner) size could be decreased, which should be quantitatively assessed in future works. Thermal inertia and flexible operation of the installation must be also carefully addressed. These effects are amplified when the residence time is increased to 10 min for the CaL process. The efficiency penalty is then clearly reduced around 1 MJ/kgCO_2 but the solids inventory is increased over a 200% up to near 700 ton. Care should be taken in this case to design and operate a system with such a large thermal inertia due to solids heat capacity. Starts-up and shuts-down would be also risky. This could be a suitable option if the CO_2 capture system is to be used in base load power plants. When power plant flexibility is required, the small inventory option allowed by the Oxy-CaL hybrid system is preferred to better accommodate the installation to load changes.

6. Conclusions

This work analyzes a novel CO_2 capture system (Oxy-CaL) based on the integration of the CaL process with partial oxy-combustion, the latter used to raise the CO_2 concentration in the flue gas thus enhancing the CaL capture efficiency. Results from thermogravimetric analysis experiments are used to simulate the hybrid capture system when integrated into a coal fired power plant (CFPP). Energy penalty and capture efficiency are analyzed for diverse Oxy-CaL systems to reach a CO_2 vol% in the flue gas in the range 30-60% and the results are compared with those obtained for the pure CaL and oxy-combustion processes.

Main highlights concluded from the study are:

- A higher CO_2 capture efficiency is achieved by means of the Oxy-CaL hybrid system while the specific energy consumption per kg of CO_2 avoided (SPECCA) is kept below 4 MJ/kg, which is a typical value usually reported for oxy-combustion or amine-based CO_2 capture systems. Thus, CO_2 capture using an Oxy-CaL system could be a potentially attractive alternative to total oxy-combustion for newly erected CFPP.
- The CaL process seems to be the most advantageous CO_2 capture process when operating under relative long solids residence time in the carbonator. However, its performance has a strong sensitivity to the carbonation rate in the solid-state diffusion controlled stage, which depends critically on temperature within the range of temperatures practically attainable in the carbonator.
- The effect of varying the carbonation temperature is more relevant when operating under long residence times due to the strong sensitivity of CaO carbonation to temperature in the solid-state diffusion controlled stage, especially for the pure CaL process.
- The higher CO_2 capture efficiency using Oxy-CaL systems allows to reduce the fresh limestone makeup flow, which leads to a reduction of energy consumption when operating under solids residence times below 7.5 minutes.
- In spite that SPECCA in the CaL process could be somewhat smaller than for the Oxy-CaL system when operating under prolonged solids residence times, the latter shows potentially important benefits regarding plant operation flexibility. Substantially

smaller amounts of solids inventory are needed in the Oxy-CaL system, which would allow a more efficient response to load changes in coal fired power plants.

In a future work, a detailed techno-economic study must be developed in order to assess quantitatively the cost of CO_2 capture by means of the Oxy-CaL system as compared to CaL and oxy-combustion and for same values of SPECCA and capture efficiency.

Acknowledgements

This work was supported by the Spanish Government Agency Ministerio de Economia y Competitividad and FEDER Funds (contracts CTQ2014-52763-C2-1-R, CTQ2014- 52763-C2-2-R and MAT2013-41233-R). We gratefully acknowledge the Functional Characterization Services of the Innovation, Technology and Research Centre of the University of Seville (CITIUS). The authors also thank VPPI-US for the AP current contract.

Notation

$[CO_2]$	average CO_2 concentration, mol/m^3	T_{calc}	calciner temperature, ºC
$[CO_2]_{eq}$	equilibrium concentration of CO_2, mol/m^3	T_{carb}	carbonator temperature, ºC
D^*_{eff}	equivalent diffusion constant, m^3/ (mol ·s)	T_{vv}	live steam temperature, ºC
E	emissions ratio after CO2 capture, kg CO_2/kWhe	t_0	time lag of TGA multicycle test, s
E_{CO2}	carbon capture efficiency	t_{FRP}	time of the carbonation fast phase, s
E_{ref}	emissions ratio before CaL, kg CO_2/kWhe	t_{max}	total carbonation time, s
E_{max}	maximum capture efficiency	v_{CO2}	CO_2 v/v concentration at CFPP outlet
F_{CO2}	mole flow rate of CO_2 in flue gas entering the carbonator, kmol/h	v_{O2}	O_2 v/v concentration at CFPP outlet
F_O	mole flow rate of fresh makeup limestone, kmol/h	W_s	solid inventory in the carbonator per MW of a typical power plant, kg
F_R	mole flow rate of CO_2 in flue gas entering the carbonator, kmol/h	$\dot{W}_{ASU}$	power consumption in the ASU, MW
F_{fg}	flue gas molar flow rate, kmol/s	$\dot{W}_{sec}$	net power production in secondary steam cycle, MW
FRP	fast reaction controlled phase	$\dot{W}_{comp,CO2}$	power consumption in CO_2 compression, MW
SDP	solid-state diffusion controlled phase	$\dot{W}_{comp,fg}$	power consumption in flue gas compression, MW
k_s	intrinsic kinetic constant m^4/ (mol ·s)	$\dot{W}_{sólid}$	power consumption in solids transport, MW
k	deactivation constant of a sorbent particle	X	carbonation degree of a CaO particle
$\dot{m}$	mass flow, kg/s	X_{ave}	average conversion of the sorbent
$\dot{m}_{CO2,calc}$	CO_2 mass flow exiting the calciner, kg/s	$X_{ave,SDP}$	average conversion of the sorbent in the diffusion phase
$\dot{m}_{gas,calc}$	Total gas mass flow exiting the calciner, kg/s	$X_{ave,FRP}$	average conversion of the sorbent in the kinetic phase
		W_s	solid inventory in the carbonator per MW of a typical power plant, kg
N_{Ca}	mol of Ca in the carbonator, mol	x_{CO2}	CO_2 Molar fraction exiting the plant

P	Pressure, bar	x_{O2}	O_2 Molar fraction exiting the plant
P_{vv}	live steam pressure, bar	$y_{CO2,in}$	CO2 molar fraction at carbonator inlet
$P_{HE,solids}$	solid-solid thermal power exchanged, MW	$y_{CO2,eq}$	CO2 molar fraction at carbonation equilibrium
$SPECCA$	energy consumption for kg CO_2 avoided, MJ/Kg CO_2	η_{boiler}	boiler efficiency
$r_{ave,SDP}$	average reaction rate in the diffusion regime, s^{-1}	η_{CFPP}	coal fire power plant efficiency
$r_{ave,FRP}$	average reaction rate in the kinetic regime, s^{-1}	η_{ref}	reference plant efficiency
S_{ave}	average surface area available for reaction, m^{-1}	η_{int}	new global efficiency (CFPP-capture system)
t	time, s	τ	average residence time in the carbonator, s

Appendix A

Figure 15 shows data on the multicycle overall CaO conversion (X_N, X_{FRP} and X_{SDP} as a function of the cycle number for the tests carried out under CaL and Oxy-CaL-45 conditions and for the diverse carbonation temperatures employed (625, 650ºC and 680ºC). Values of the deactivation rate constant and residual conversion obtained from the fittings of Eq. 1 to experimental data are also shown in Table 4.

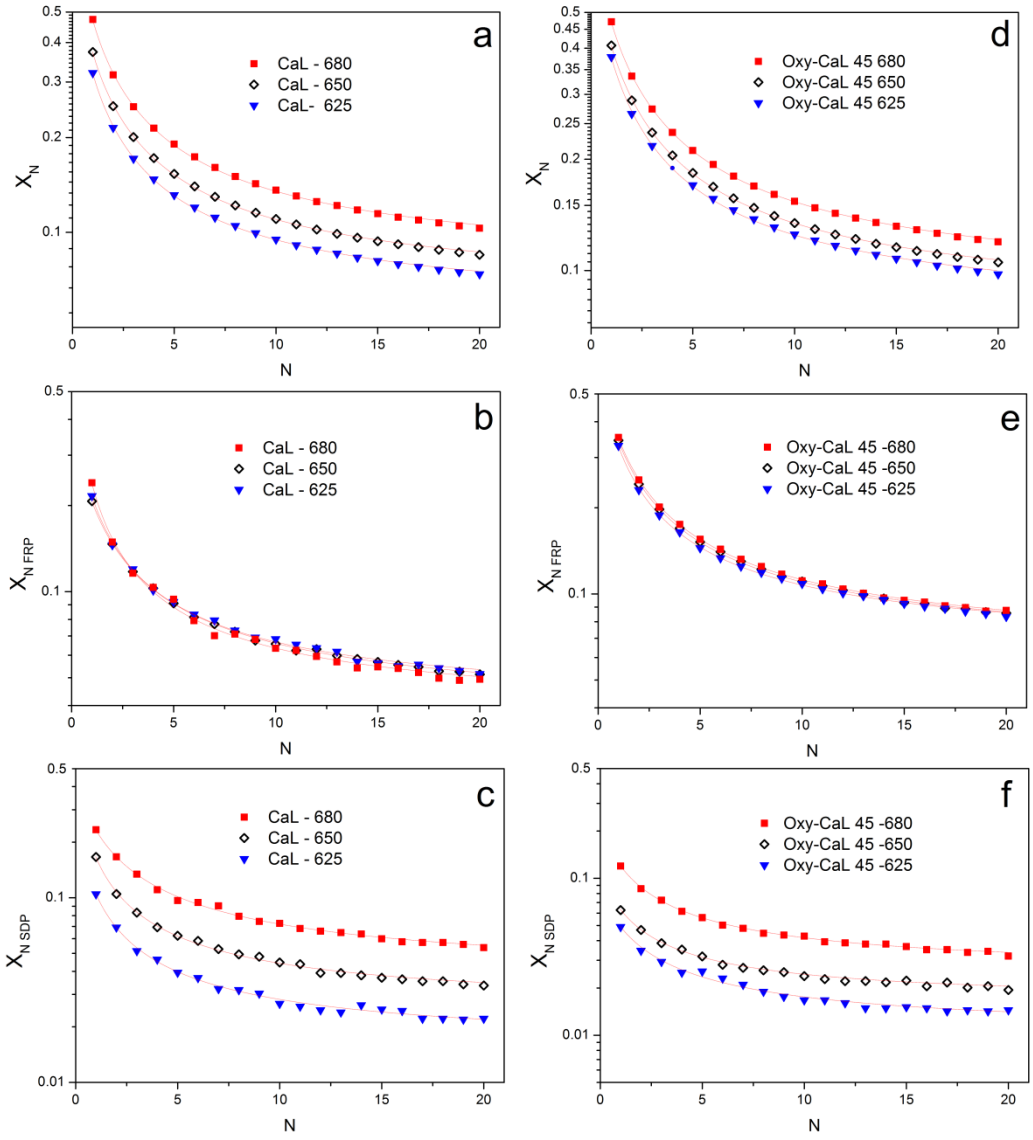

Figure 15. (a, d) Overall CaO conversion versus the cycle number for carbonation/calcination cycles carried out under CaL and Oxy-CaL-45 conditions. (b, e) Conversion in the fast reaction controlled phase. (c, f) Conversion in the solid-state diffusion controlled phase. Carbonation is carried out under 15% vol CO_2 (CaL conditions) and 45% vol CO_2 (Oxy-CaL-45 conditions) at 625ºC, 650ºC and 680ºC as indicated. Calcination is performed at 950ºC (70% CO_2/30% air vol/vol) in all the tests.

Table 4: Values of the deactivation rate constant κ and residual conversion X_r obtained from the best fits of Eq. (1) to TGA experimental data for carbonation at different temperatures (625, 650, and 680ºC) and CO_2 concentrations (15% vol in the CaL tests; 30%, 45%, and 60% vol in the Oxy-CaL tests).

T carb =625ºC		**CaL-625**	**Oxy-CaL30-625**	**Oxy-CaL45-625**	**Oxy-CaL60-625**
$X_{overall}$	X_1	0.321	0.338	0.378	0.400
	κ	0.753	0.665	0.675	0.623
	X_r	0.053	0.067	0.072	0.077
	R_{sqr}	0.999	0.999	0.999	0.999
X_{FRP}	X_1	0.216	0.260	0.329	0.350
	κ	0.737	0.697	0.683	0.647
	X_r	0.038	0.056	0.062	0.067
	R_{sqr}	0.999	0.998	0.999	0.999
X_{SDP}	X_1	0.105	0.078	0.049	0.050
	κ	0.792	0.573	0.615	0.464
	X_r	0.015	0.011	0.010	0.0103
	R_{sqr}	0.997	0.996	0.990	0.994
T carb =650ºC		**CaL-650**	**Oxy-CaL30-650**	**Oxy-CaL45-650**	**Oxy-CaL60-650**
$X_{overall}$	X_1	0.373	0.388	0.407	0.425
	κ	0.731	0.667	0.651	0.633
	X_r	0.061	0.070	0.076	0.081
	R_{sqr}	0.999	0.999	0.999	0.999
X_{FRP}	X_1	0.207	0.293	0.344	0.374
	κ	0.660	0.661	0.641	0.674
	X_r	0.037	0.053	0.060	0.068
	R_{sqr}	0.999	0.999	0.999	0.998
X_{SDP}	X_1	0.166	0.095	0.063	0.051
	κ	0.828	0.686	0.711	0.633
	X_r	0.025	0.016	0.016	0.014
	R_{sqr}	0.998	0.998	0.993	0.980
T carb =680ºC		**CaL-680**	**Oxy-CaL30-680**	**Oxy-CaL45-680**	**Oxy-CaL60-680**
$X_{overall}$	X_1	0.474	0.472	0.472	0.474
	κ	0.737	0.681	0.636	0.636
	X_r	0.074	0.081	0.085	0.086
	R_{sqr}	0.999	0.999	0.999	0.999
X_{FRP}	X_1	0.240	0.299	0.352	0.391
	κ	0.876	0.716	0.630	0.673
	X_r	0.037	0.057	0.060	0.066
	R_{sqr}	0.997	0.999	0.999	0.999
X_{SDP}	X_1	0.233	0.173	0.120	0.083
	κ	0.609	0.627	0.655	0.478
	X_r	0.037	0.025	0.025	0.020
	R_{sqr}	0.998	0.999	0.999	0.990

Appendix B

Table 5: Inputs and results of diverse CO_2 capture systems for the base case.

	parameter	Reference CFFP (air combustion)	oxy-combustion	CaL	Oxy-CaL 30	Oxy-CaL 45	Oxy-CaL 60
CFPP	$\dot{m}_{coal}\ (kg/s)$	42.20	55.05	42.20	46.10	47.50	48.15
	$\dot{m}_{air}\ (kg/s)$	475	-	475	208.90	100.20	43.54
	$\dot{m}_{O2}\ (kg/s)$	-	136.91	-	68.85	96.35	110.503
	γ_{fg}	-	0.78	-	0.63	0.72	0.75
	$F_{fg}\ (kmol/s)$	17.12	3.85	17.12	10.13	7.25	5.74
	$F_{CO2}\ (kmol/s)$	2.60	3.39	2.60	2.84	2.93	2.96
	v_{CO2}	0.15	0.89	0.15	0.30	0.45	0.60
	v_{O2}	0.023	0.025	0.023	0.025	0.025	0.025
	η_{boiler}	0.90	0.90	0.90	0.90	0.90	0.90
	η_{CFPP}	0.3777	0.2872	0.3777	0.3517	0.3437	0.3374
	$net\ work\ (MW)$	490.47	488.80	490.47	498.30	502.30	499.75
	$Penalty$	-	**9.05%**	**-**	**2.60%**	**3.40%**	**4.03%**
	$SPECCA$ (MJ/kg_{CO2})	-	**4.06**	**-**	**0.94**	**1.25**	**1.50**
CaL	F_R/F_{CO2}	-	-	15	15	15	15
	F_0/F_{CO2}	-	-	0.05	0.05	0.05	0.05
	$\tau\ (min)$	-	-	3.05	2.79	2.71	2.68
	$T_{calc}\ (ºC)$	-	-	950	950	950	950
	$T_{carb}\ (ºC)$	-	-	650	650	650	650
	E_{CO2}	-		0.827	0.950	0.976	0.981
	$\dot{m}_{coal}\ (kg/s)$	-	-	18.48	22.34	23.40	23.84
	$\dot{m}_{O2}\ (kg/s)$	-	-	48.00	58.41	61.00	62.49
	γ_{fg}	-	-	0.7	0.7	0.7	0.7
	$\dot{m}_{gas,calc}\ (kg/s)$	-	-	165.07	203.6	214	218.34
	$\dot{m}_{CO2,calc}\ (kg/s)$	-	-	150.45	185.70	195.40	199.19
	x_{CO2}	-	-	0.030	0.019	0.017	0.026
	x_{O2}	-	-	0.028	0.032	0.042	0.058
	$P_{HE,solids}$	-	-	640.92	697.60	717.80	727.29
	$\dot{W}_{sec}\ (MW)$	-	-	75.80	113.90	126.46	130.88
	$\dot{W}_{solids}\ (MW)$	-	-	45.70	49.72	51.16	51.82
	$\dot{W}_{ASU}\ (MW)$	-	-	34.56	42.05	43.92	44.99
	$\dot{W}_{comp,CO2}\ (MW)$	-	-	57.55	71.01	74.59	75.20
	$\dot{W}_{comp,FG}\ (MW)$	-	-	12.53	7.27	4.90	3.66
	η_{int}	-	-	0.3030	0.2909	0.2882	0.2853
	$Penalty$	-	-	**7.43%**	**6.04%**	**5.48%**	**5.27%**
	$SPECCA$ (MJ/kg_{CO2})	-	-	**3.28**	**2.63**	**2.37**	**2.29**
Total	$\dot{m}_{coal,total}$	-	-	60.68	68.44	70.90	71.99
	$Penalty_{total}$	-	**9.05%**	**7.47%**	**8.68%**	**8.95%**	**9.24%**
	$SPECCA_{total}$ (MJ/kg_{CO2})	-	**4.06**	**3.28**	**3.56**	**3.62**	**3.79**

References

[1] IEA. Energy Technology Perspectives 2012. 2012. doi:10.1787/energy_tech-2012-en.

[2] Tokimatsu K, Konishi S, Ishihara K, Tezuka T, Yasuoka R, Nishio M. Role of innovative technologies under the global zero emissions scenarios. Appl Energy 2016;162:1483–93. doi:10.1016/j.apenergy.2015.02.051.

[3] Goto K, Yogo K, Higashii T. A review of efficiency penalty in a coal-fired power plant with post-combustion CO_2 capture. Appl Energy 2013;111:710–20. doi:10.1016/j.apenergy.2013.05.020.

[4] Bevan N, Boston A. CCS Forum Report. 2016.

[5] Wang M, Lawal A, Stephenson P, Sidders J, Ramshaw C, Hill W, et al. Post-combustion CO_2 capture with chemical absorption: A state-of-the-art review. Chem Eng Res Des 2011;89:1609–24. doi:10.1016/j.cherd.2010.11.005.

[6] Perejon A, Romeo LM, Lara Y, Lisbona P, Valverde JM. The Calcium-Looping technology for CO_2 capture: On the important roles of energy integration and sorbent behavior. Appl Energy 2015;162:787–807. doi:10.1016/j.apenergy.2015.10.121.

[7] Politecnico di Milano – Alstom UK (CAESAR project). European best practice guidelines for assessment of CO_2 capture technologies. 2011.

[8] Aaron D, Tsouris C. Separation of CO_2 from Flue Gas: A Review. Sep Sci Technol 2005;40:321–48. doi:10.1081/SS-200042244.

[9] Wang M, Joel AS, Ramshaw C, Eimer D, Musa NM. Process intensification for post-combustion CO_2 capture with chemical absorption: A critical review. Appl Energy 2015;158:275–91. doi:10.1016/j.apenergy.2015.08.083.

[10] Luis P. Use of monoethanolamine (MEA) for CO_2 capture in a global scenario: Consequences and alternatives. Desalination 2016;380:93–9. doi:10.1016/j.desal.2015.08.004.

[11] Rey A, Gouedard C, Ledirac N, Cohen M, Dugay J, Vial J, et al. Amine degradation in CO_2 capture. 2. New degradation products of MEA. Pyrazine and alkylpyrazines: Analysis, mechanism of formation and toxicity. Int J Greenh Gas Control 2013;19:576–83. doi:10.1016/j.ijggc.2013.10.018.

[12] Shimizu T, Hirama T, Hosoda H, Kitano K, Inagaki M, Tejima K. A Twin Fluid-Bed Reactor for Removal of CO_2 from Combustion Processes. Chem Eng Res Des 1999;77:62–8. doi:10.1205/026387699525882.

[13] Ortiz C, Valverde JM, Chacartegui R. Energy Consumption for CO_2 Capture by means of the Calcium Looping Process: A Comparative Analysis using Limestone, Dolomite, and Steel Slag. Energy Technol 2016:1–12. doi:10.1002/ente.201600390.

[14] Ströhle J, Junk M, Kremer J, Galloy A, Epple B. Carbonate looping experiments in a 1 MWth pilot plant and model validation. Fuel 2014;127:13–22. doi:10.1016/j.fuel.2013.12.043.

[15] Arias B, Diego ME, Abanades JC, Lorenzo M, Diaz L, Martínez D, et al. Demonstration of steady state CO_2 capture in a 1.7MWth calcium looping pilot. Int J Greenh Gas Control 2013;18:237–45. doi:10.1016/j.ijggc.2013.07.014.

[16] Hanak DP, Anthony EJ, Manovic V. A review of developments in pilot-plant testing and modelling of calcium looping process for CO_2 capture from power generation systems. Energy Environ Sci 2015;8:2199–249. doi:10.1039/C5EE01228G.

[17] Abanades JC, Grasa G, Alonso M, Rodriguez N, Anthony EJ, Romeo LM. Cost structure of a postcombustion CO_2 capture system using CaO. Environ Sci Technol 2007;41:5523–7. doi:10.1021/es070099a.

[18] Scheffknecht G, Al-Makhadmeh L, Schnell U, Maier J. Oxy-fuel coal combustion-A review of the current state-of-the-art. Int J Greenh Gas Control 2011;5:16–35. doi:10.1016/j.ijggc.2011.05.020.

[19] Escudero AI, Espatolero S, Romeo LM, Lara Y, Paufique C, Lesort A-L, et al. Minimization of CO_2 capture energy penalty in second generation oxy-fuel power plants. Appl Therm Eng 2016;103:274–81. doi:10.1016/j.applthermaleng.2016.04.116.

[20] Jin B, Zhao H, Zheng C. Thermoeconomic cost analysis of CO_2 compression and purification unit in oxy-combustion power plants Bo. Energy 2015;83:416–30. doi:10.1016/j.energy.2015.02.039.

[21] Posch S, Haider M. Optimization of CO_2 compression and purification units (CO_2CPU) for CCS power plants. Fuel 2012;101:254–63. doi:10.1016/j.fuel.2011.07.039.

[22] Escudero AI, Espatolero S, Romeo LM. Oxy-combustion power plant integration in an oil refinery to reduce CO_2 emissions. Int J Greenh Gas Control 2016;45:118–29. doi:10.1016/j.ijggc.2015.12.018.

[23] Kather A, Scheffknecht G. The oxycoal process with cryogenic oxygen supply. Naturwissenschaften 2009;96:993–1010. doi:10.1007/s00114-009-0557-2.

[24] Vega F, Sanna A, Maroto-Valer MM, Navarrete B, Abad-Correa D. Study of the MEA degradation in a CO_2 capture process based on partial oxy-combustion approach. Int J Greenh Gas Control 2016;54:160–7. doi:10.1016/j.ijggc.2016.09.007.

[25] Ylätalo J, Parkkinen J, Ritvanen J, Tynjälä T, Hyppänen T. Modeling of the oxy-combustion calciner in the post-combustion calcium looping process. Fuel 2013;113:770–9. doi:10.1016/j.fuel.2012.11.041.

[26] Martínez I, Grasa G, Murillo R, Arias B, Abanades JC. Modelling the continuous calcination of $CaCO_3$ in a Ca-looping system. Chem Eng J 2013;215–216:174–81. doi:10.1016/j.cej.2012.09.134.

[27] Koga N, Criado JM. The influence of mass transfer phenomena on the kinetic analysis for the thermal decomposition of calcium carbonate by constant rate thermal analysis (CRTA) under vacuum. Int J Chem Kinet 1998;30:737–44. doi:10.1002/(SICI)1097-4601(1998)30:10<737::AID-KIN6>3.0.CO;2-W.

[28] Alonso M, Criado Y a., Abanades JC, Grasa G. Undesired effects in the determination of CO_2 carrying capacities of CaO during TG testing. Fuel 2014;127:52–61. doi:10.1016/j.fuel.2013.08.005.

[29] Grasa G, Murillo R, Alonso M, Abanades JC. Application of the random pore model to the carbonation cyclic reaction. AIChE J 2009;55:1246–55. doi:10.1002/aic.11746.

[30] Bhatia SK, Perlmutter DD. Effect of the product layer on the kinetics of the carbon dioxide-lime reaction. AIChE J 1983;29:79–86. doi:10.1002/aic.690290111.

[31] Sun Z, Luo S, Qi P, Fan LS. Ionic diffusion through Calcite (CaCO 3) layer during the

reaction of CaO and CO_2. Chem Eng Sci 2012;81:164–8. doi:10.1016/j.ces.2012.05.042.

[32] Bhatia SK, Perlmutter DD. Effect of the product layer on the kinetics of the CO_2-lime reaction. AIChE J 1983;29:79–86. doi:10.1002/aic.690290111.

[33] Anderson TF. Self-diffusion of carbon and oxygen in calcite by isotope exchange with carbon dioxide. J Geophys Res 1969;74:3918–32. doi:10.1029/JB074i015p03918.

[34] Grasa GS, Abanades JC. CO_2 Capture Capacity of CaO in Long Series of Carbonation/Calcination Cycles. Ind Eng Chem Res 2006;45:8846–51. doi:10.1021/ie0606946.

[35] Valverde JM. A model on the CaO multicyclic conversion in the Ca-looping process. Chem Eng J 2013;228:1195–206. doi:10.1016/j.cej.2013.05.023.

[36] Blamey J, Anthony EJ, Wang J, Fennell PS. The calcium looping cycle for large-scale CO_2 capture. Prog Energy Combust Sci 2010;36:260–79. doi:10.1016/j.pecs.2009.10.001.

[37] Zhu Y, Wu S, Wang X. Nano CaO grain characteristics and growth model under calcination. Chem Eng J 2011;175:512–8. doi:10.1016/j.cej.2011.09.084.

[38] Ortiz C, Chacartegui R, Valverde J, Becerra J, Perez-Maqueda L. A new model of the carbonator reactor in the calcium looping technology for post-combustion CO_2 capture. FUEL 2015;160:328–38. doi:10.1016/j.fuel.2015.07.095.

[39] USA National Energy Technology Laboratory. Detailed Coal Specifications Quality Guidelines for Energy System Studies. 2012.

[40] Romano MC. Ultra-high CO_2 capture efficiency in CFB oxyfuel power plants by calcium looping process for CO_2 recovery from purification units vent gas. Int J Greenh Gas Control 2013;18:57–67. doi:10.1016/j.ijggc.2013.07.002.

[41] Zhang X, Bauer C, Mutel CL, Volkart K. Life Cycle Assessment of Power-to-Gas: Approaches, system variations and their environmental implications. Appl Energy 2017;190:326–38. doi:10.1016/j.apenergy.2016.12.098.

[42] Perez-Fortes M, Schoneberger JC, Boulamanti A, Tzimas E. Methanol synthesis using captured CO_2 as raw material: Techno-economic and environmental assessment. Appl Energy 2016;161:718–32. doi:10.1016/j.apenergy.2015.07.067.

[43] Pei X, He B, Yan L, Wang C, Song W, Song J. Process simulation of oxy-fuel combustion for a 300 MW pulverized coal-fired power plant using Aspen Plus. Energy Convers Manag 2013;76:581–7. doi:10.1016/j.enconman.2013.08.007.

[44] Romano M, Martínez I, Murillo R, Arstad B. Guidelines for modeling and simulation of Ca-looping processes. 2012.

[45] Martínez I, Murillo R, Grasa G, Abanades JC. Integration of a Ca-looping system for CO_2 capture in an existing power plant. Energy Procedia 2011;4:1699–706. doi:10.1016/j.egypro.2011.02.043.

[46] Hanak DP, Powell D, Manovic V. Techno-economic analysis of oxy-combustion coal-fired power plant with cryogenic oxygen storage. Appl Energy 2017;191:193–203. doi:10.1016/j.apenergy.2017.01.049.

[47] Ortiz C, Chacartegui R, Valverde JM, Becerra JA. A new integration model of the

calcium looping technology into coal fired power plants for CO_2 capture. Appl Energy 2016;169:408–20. doi:10.1016/j.apenergy.2016.02.050.

[48] Ylätalo J, Ritvanen J, Tynjälä T, Hyppänen T. Model based scale-up study of the calcium looping process. Fuel 2014;115:329–37. doi:10.1016/j.fuel.2013.07.036.

[49] Romano MC. Modeling the carbonator of a Ca-looping process for CO_2 capture from power plant flue gas. Chem Eng Sci 2012;69:257–69. doi:10.1016/j.ces.2011.10.041.

[50] Vorrias I, Atsonios K, Nikolopoulos A, Nikolopoulos N, Grammelis P, Kakaras E. Calcium looping for CO_2 capture from a lignite fired power plant. Fuel 2013;113:826–36. doi:10.1016/j.fuel.2012.12.087.

[51] Dieter H, Bidwe AR, Varela-duelli G, Charitos A, Hawthorne C. Development of the calcium looping CO_2 capture technology from lab to pilot scale at IFK , University of Stuttgart. Fuel 2014;127:23–37. doi:10.1016/j.fuel.2014.01.063.

[52] Charitos A, Rodríguez N, Hawthorne C, Alonso M, Zieba M, Arias B, et al. Experimental Validation of the Calcium Looping CO_2 Capture Process with Two Circulating Fluidized Bed Carbonator Reactors. Ind Eng Chem Res 2011;50:9685–95. doi:10.1021/ie200579f.

[53] Kunii D, Levenspiel O. The K-L reactor model for circulating fluidized beds. Chem Eng Sci 2000;55:4563–70. doi:10.1016/S0009-2509(00)00073-7.

[54] Kunii D, Levenspiel O. Circulating fluidized-bed reactors. Chem Eng Sci 1997;52:2471–82. doi:10.1016/S0009-2509(97)00066-3.

[55] Edwards SEB, Materić V. Calcium looping in solar power generation plants. Sol Energy 2012;86:2494–503. doi:10.1016/j.solener.2012.05.019.

[56] Martínez I, Grasa G, Parkkinen J, Tynjälä T, Hyppänen T, Murillo R, et al. Review and research needs of Ca-Looping systems modelling for post-combustion CO_2 capture applications. Int J Greenh Gas Control 2016;50:271–304. doi:10.1016/ j.ijggc.2016.04.002.

[57] Hanak DP, Kolios AJ, Manovic V. Comparison of probabilistic performance of calcium looping and chemical solvent scrubbing retrofits for CO_2 capture from coal-fired power plant. Appl Energy 2016;172:323–36. doi:10.1016/j.apenergy.2016.03.102.